Published in final edited form as:

Neuron. 2018 February 07; 97(3): 611–625.e5. doi:10.1016/j.neuron.2018.01.037.

Precisely-timed nicotinic activation drives SST inhibition in neocortical circuits

Joanna Urban-Ciecko[1,2], **Jean-Sebastien Jouhanneau**[3,4], **Stephanie E. Myal**[1], **James F.A. Poulet**[3,4], and **Alison L. Barth**[1,*]

[1]Department of Biological Sciences and Center for the Neural Basis of Cognition, Carnegie Mellon University, Pittsburgh PA 15213 [2]Department of Molecular and Cellular Neurobiology, Nencki Institute of Experimental Biology, Pasteur str. 3, 02-093 Warsaw, Poland [3]Department of Neuroscience, Max Delbrück Center for Molecular Medicine (MDC), Berlin-Buch, Robert-Rössle-Str. 10, 13092 Berlin, Germany [4]Cluster of Excellence NeuroCure, Neuroscience Research Center, Charité-Universitätsmedizin Berlin, Charitéplatz 1, 10117 Berlin, Germany

Summary

Sleep, waking, locomotion, and attention are associated with cell-type specific changes in neocortical activity. The effect of brain state on circuit output requires understanding of how neuromodulators influence specific neuronal classes and their synapses, with normal patterns of neuromodulator release from endogenous sources. We investigated the state-dependent modulation of a ubiquitous feedforward inhibitory motif in mouse sensory cortex, local pyramidal (Pyr) inputs onto somatostatin-expressing (SST) interneurons. Paired whole-cell recordings in acute brain slices and *in vivo* showed that Pyr-to-SST synapses are remarkably weak, with failure rates approaching 80%. Pharmacological screening revealed that cholinergic agonists uniquely enhance synaptic efficacy. Brief, optogenetically-gated acetylcholine release dramatically enhanced Pyr-to-SST input, via nicotinic receptors and presynaptic PKA signalling. Importantly, endogenous acetylcholine release preferentially activated nicotinic, not muscarinic receptors, thus differentiating drug effects from endogenous neurotransmission. Brain state, synapse-specific unmasking of synapses may be a powerful way to functionally rewire cortical circuits dependent on behavioral demands.

Introduction

Slow-wave sleep, wake, locomotion, and attention are associated with changes in neocortical activity, with characteristic effects on different classes of neurons (Alitto and Dan, 2012;

*To whom correspondence should be addressed: barth@cmu.edu.

Author contributions: Conceptualization, JUC, ALB, JFAP; Methodology, JUC, ALB, JSJ, JFAP; Investigation, *ex vivo*, JUC, SEM; *in vivo*, JSJ; Writing – original draft, JUC and ALB; Writing – review and editing, JUC, ALB, JSJ, JFAP; Funding acquisition, ALB, JUC, and JFAP; Resources, ALB and JFAP; Supervision, ALB and JFAP.

Contact for reagent and resource sharing

Further information and requests for resources and reagents should be directed to and will be fulfilled by the Lead Contact, Alison L. Barth (barth@cmu.edu)

Declaration of Interests

The authors have declared that no competing interest exists.

Garcia-Junco-Clemente et al., 2017; Gentet et al., 2012; Pakan et al., 2016; Polack et al., 2013). For example, attention and arousal are associated with the desynchronization of cortical activity (McGinley et al., 2015; Poulet and Petersen, 2008), an effect that has been generally attributed to altered inhibition (Manseau et al., 2010; Renart et al., 2010; Trevino, 2016) and enhanced thalamic drive (Poulet et al., 2012). Understanding how brain state can modulate circuit function will require an understanding of how neuromodulators influence specific neuronal classes and the synapses that link them together. Importantly, this should be done in the context of phasic, focal patterns of neuromodulator release from endogenous sources, rather than broad and prolonged pharmacological activation.

Here we investigate the state-dependent modulation of a common synaptic motif in neocortical circuits, the excitatory synapse from pyramidal neurons (Pyr) to SST interneurons, a ubiquitous architecture hypothesized to underlie feedback inhibition that can scale overall levels of firing across differing levels of sensory input to the neocortex (Kapfer et al., 2007; Miller, 2016; Silberberg and Markram, 2007). It has been proposed that this motif is critical to trigger inhibition through SST neurons to prevent recurrent or runaway activity in the circuit.

Although synaptic connections between Pyr and SST neurons are common – a consensus of studies show that ~30% of Pyr neurons will be connected to a nearby SST neuron (Jiang et al., 2015; Kapfer et al., 2007; Levy and Reyes, 2012; Pala and Petersen, 2015; Silberberg and Markram, 2007) – these connections are remarkably weak and often require multiple presynaptic spikes delivered at high frequency to be detected (Berger et al., 2010; Fanselow et al., 2008; Kapfer et al., 2007; Pala and Petersen, 2015; Silberberg and Markram, 2007). Moreover, early studies were carried out under idealized conditions designed to maximize neurotransmitter release, and the firing frequencies (prolonged bursts at 20–70 Hz) employed are extreme, outside the range of those normally observed during awake activity (Barth and Poulet, 2012). The plausibility of disynaptic inhibition through SST neurons for effective feedback inhibition and gain control in neocortical circuits *in vivo* remains open.

We therefore sought to determine the conditions under which the brain makes use of this ubiquitous synaptic motif. Both *in vivo* and in acute brain slices with physiological levels of Ca^{2+} (Borst, 2010; Somjen, 2004), we find that in superficial layers of somatosensory cortex, Pyr-SST synapses may be both more ubiquitous but also weaker than previously reported, with single-spike failure rates that approach 80%, and can be undetectable in 20% of verified connected pairs (i.e., 100% failure rate to single spikes).

What are the conditions under which local excitatory inputs can engage SST inhibition? We find that synaptic efficacy at Pyr-SST connections is uniquely enhanced by cholinergic signaling, a critical neuromodulatory pathway that has been implicated in arousal, attention, and also cognitive disorders such as Alzheimer's disease. Increased synaptic strength at Pyr-SST synapses can be observed both with pharmacological activation of acetylcholine receptors (AChRs) as well as with the delivery of ACh from endogenous sources matched to normal patterns of cholinergic neural firing. These effects are mediated by presynaptic nicotinic AChRs (nAChRs) and the activation of PKA signaling pathways at Pyr-SST inputs, and require a delay between cholinergic release and the enhancement of release probability.

Cholinergic enhancement of excitatory synaptic strength at SST neurons is synapse-specific, as it was absent at L2 Pyr to Pyr synapses and Pyr to parvalbumin-expressing (PV) interneurons. Thus, local excitatory input to SST neurons is selectively enhanced during the cholinergic modulation of network activity. Our findings indicate that brain state can selectively alter network function through the input-specific modulation of specific synaptic motifs, and provide a potential mechanism by which attention can decorrelate neural activity and control the gain of local circuits through increased inhibition.

Results

Pyr inputs to SST neurons are weak and have a high failure rate

Brain slice and *in vivo* studies indicate that pyramidal cells in the neocortex are reciprocally connected to nearby SST neurons with high probability, with estimates typically ranging from 20–30% for Pyr to SST connections and >60% SST to Pyr connectivity (Urban-Ciecko and Barth, 2016), data that suggest SST neurons could provide temporally precise feedback inhibition. Although the recruitment and impact of SST-mediated inhibition has been extensively modeled (Krishnamurthy et al., 2015; Markram et al., 2015; Potjans and Diesmann, 2014; Vierling-Claassen et al., 2010), the weak synaptic properties of Pyr to SST connections indicate that this motif might be difficult to engage except for under very specialized regimes, where individual pyramidal neurons fire multiple spikes at non-physiologically high frequencies (Berger et al., 2010; Hilscher et al., 2017; Kapfer et al., 2007; Silberberg and Markram, 2007). To quantify these limitations and better understand when SST neurons can be engaged for temporally-precise inhibition, we examined Pyr to SST synapses under a variety of stimulation conditions, both in acute brain slices and *in vivo*.

For slice recordings, we adjusted extracellular Ca^{2+} levels to values observed in CSF (~1 mM; (Somjen, 2004), and enabled some slow oscillatory network activity to be present, conditions that approximate the quiet resting state *in vivo* (Sanchez-Vives and McCormick, 2000). Using a 10 spike train delivered at 20 Hz, we identified synaptically connected Pyr-SST pairs in layer 2 (L2) of mouse somatosensory (barrel) cortex and calculated the first-spike mean amplitude and failure rate (Figure 1). Because neocortical neurons typically fire at very low rates (Barth and Poulet, 2012), analysis of synaptic responses to the initial spike is a reasonable way to assess Pyr input strength to SST neurons under normal behavioral conditions.

Synaptic strength was remarkably weak under these conditions. Mean EPSP amplitudes, calculated after the first spike (10-sweep average), were nearly 5-fold lower than some previously reported values (Jiang et al., 2015; Pala and Petersen, 2015): 0.18±0.02 mV (range 0–1.67, n=90). Mean failure rates across all cells were 79±2%, indicating that EPSP responses to a single presynaptic spike are the exception rather than the rule for these local excitatory inputs. Indeed, we found that 20% of connected pairs would have been missed by a single-spike analysis (see for example (Jiang et al., 2015; Pala and Petersen, 2015) due to 100% failure rates for the initial spike at these connections. Importantly, increasing extracellular Ca^{2+} and suppressing background activity in the slice was sufficient to reveal connections that were otherwise difficult to detect (Figure 1A, D, E). Delivery of a

naturalistic spike train (previously recorded from L2 Pyr neurons *in vivo)* that included spike bursts recorded did not alter failure rates in acute brain slices (Figure 1B).

Connection probability was determined by assessments of responses throughout the 10 spike train. Direct synaptic connections from Pyr to SST neurons were found in 53% of tested pairs (220/411), and this probability did not change when Ca^{2+} levels were higher, since the strong facilitation observed enabled us to accurately classify neurons as connected even if single-spike failure rates were high. Connection probabilities for Pyr-SST pairs were similar for *in vivo* recordings, using spike-train stimulation to detect weak inputs. Using multiple trial averaging and analysis of responses across a prolonged spike train, we found that 46.6% (7/15) tested Pyr cells were synaptically connected to nearby SST neurons (Figure 1C).

Within-cell comparisons of Pyr-SST synaptic efficacy recorded in both normal (physiological, 1 mM) and then elevated (2.5 mM) extracellular Ca^{2+} levels showed that EPSP amplitudes were significantly larger (normal 0.53±0.34 mV vs elevated 0.24±0.2 mV; n=8, p=0.02) and single-spike failure rates tended to be lower (normal 58±1% vs elevated 81±6%; p=0.08; Wilcoxin test, Figure 1D,E).

How do these values from acute brain slices compare to synaptic performance of Pyr to SST inputs *in vivo*? Although high levels of spontaneous subthreshold activity during *in vivo* recordings made it challenging to assess synaptic strength and response failures, we found that during hyperpolarized periods of synaptic quiescence (i.e. Downstates) that isolated-spike EPSP failures occurred in nearly three-quarters of trials (73±4%, n=6). This value was similar to that recorded in acute brain slices (Figure 1D,E). Thus, these data indicate that the frequency of Pyr to SST connections are common and failure rates are high, and that our recording conditions for acute brain slices recapitulate what has been observed *in vivo*.

Cholinergic enhancement of Pyr-SST inputs

The energetic costs of building and maintaining this ubiquitous synaptic motif across the neocortex is at odds with the weak and unreliable responses observed in our recordings. We hypothesized that there might be specific conditions under which local excitatory inputs might be revealed. Initially we observed that the PKA activator forskolin strongly potentiated synaptic efficacy, as has been observed at other central synapses (Seino and Shibasaki, 2005), suggesting that neuromodulators might be important in enhancing transmission (Figure 2).

The effects of seven different potential neuromodulators on Pyr-SST synaptic efficacy were examined: carbachol, a broad-spectrum cholinergic agonist (Khiroug et al., 2003; Yan et al., 1995); adenosine, since activated glial cells can release adenosine and presynaptic adenosine receptors can enhance synaptic strength (van Aerde et al., 2015); endocannabinoid inhibitors, since the high basal firing of SST neurons in the slice could generate constitutive activation of presynaptic CB1 receptors or depolarization-induced suppression of excitation (DSE; (Kano et al., 2009)); DHPG, a metabotropic glutamate receptor (mGluR) agonist (Anwyl, 1999; Chavis et al., 1995; Cochilla and Alford, 1998); serotonin (Dawson et al., 2001); CY, dopamine receptor type 1 agonists (Surmeier et al., 2007) and norepinephrine (Kawaguchi and Shindou, 1998) (Figure 2). To accurately compare EPSP amplitude before

and after drug application, the resting membrane potential of the postsynaptic SST neuron was matched to the baseline value to suppress potential changes in resting membrane potential and spontaneous firing activity in the SST cell. Within-cell comparisons revealed that only carbachol significantly enhanced both EPSP amplitude and reduced failure rates (Figure 2, 3A–C).

Synaptic strength is often evaluated by looking at the paired pulse ratio (PPR) for sequential stimuli (amplitude of 2nd/amplitude of 1st response). However, because initial responses were frequently 0 at Pyr-SST synapses, this was difficult to calculate for all connected pairs. When possible to calculate, PPR was 4.04±2.6 under baseline conditions, and carbachol had a strong effect in reducing the PPR, showing a 4-fold decrease (PPR=0.9±0.32) after drug application (n=4). The carbachol-dependent reduction in PPR, together with the decreased failure rate, suggested a presynaptic locus for modulation at the Pyr to SST synapse.

Which AChR-subtype mediates the increase in Pyr-SST synaptic efficacy? Cholinergic receptors can be nicotinic (ligand-gated cation channels; nAChRs), or muscarinic (metabotropic G-protein coupled receptors; mAChRs). ACh has been hypothesized to selectively alter synaptic transmission at some neocortical synapses (Arroyo et al., 2014; Gil et al., 1997; Gioanni et al., 1999; McGehee et al., 1995) and presynaptic nAChRs can enhance transmission at mossy fiber inputs to CA3 neurons in the hippocampus (Cheng and Yakel, 2015a, b). Pharmacological analysis to selectively block either nAChR or mAChRs revealed that nicotinic, but not muscarinic, receptors were required to enhance Pyr to SST connection strength (Figure 3D–G). The carbachol effect of enhancing EPSP efficacy was blocked in the presence of the nAChR antagonist mecamylamine (amplitude baseline 0.20±0.07 mV vs carbachol + mecamylamine 0.26±0.10, failure rate baseline 0.72±0.07 vs carbachol + mecamylamine 0.72±0.07; n=6, p=0.84 and p=0.99, respectively; Figure 3D, E). In contrast, the carbachol-dependent increase in Pyr-SST input strength was maintained with bath application of the mAChR-selective antagonist atropine, indicating mAChRs were not involved (amplitude baseline 0.13±0.06 mV vs carbachol+atropine 0.28±0.06, failure rates baseline 0.80±0.05 vs carbachol+atropine 0.63±0.04, n=8, p=0.0007 and p=0.03, respectively; Figure 3F,G).

Although we attempted to augment Pyr to SST synaptic strength using bath application of nicotine, we did not observe any effect under these conditions (data not shown). This is likely due to the rapid desensitization of nAChRs, which has been well-documented in other systems (Auerbach and Akk, 1998; Cachelin and Colquhoun, 1989; Ochoa et al., 1989).

Endogenous ACh release is sufficient to awaken Pyr-SST synapses

Prolonged bath application of cholinergic agonists is markedly different from the manner in which ACh is released during normal brain function. Especially in an actively firing network, cholinergic effects on diverse cell types across a circuit can make it difficult to differentiate direct and indirect effects. In addition, bath application of agonists results in broad spatial and temporal activation that may not reflect the precision of endogenous acetylcholine release.

To determine whether endogenous release of ACh might be sufficient to elicit the same increase in Pyr to SST synaptic strength, we used optogenetic activation of cholinergic terminals in the neocortex. *In vivo* recordings from cholinergic neurons in the basal forebrain indicate that these neurons may fire at a low frequency in quiet, awake animals (~4 Hz; (Hangya et al., 2015; Hassani et al., 2009; Lee et al., 2005) and may be synchronously activated to fire a single, precisely-timed spike when a behaviorally relevant cue is present (Hangya et al., 2015). With this in mind, we sought to determine what the temporal constraints of cholinergic modulation of Pyr to SST inputs were.

SST neurons were virally labeled in a SST-Cre x ChAT-ChR2 transgenic mouse to enable light-evoked ACh release, and acute brain slices were prepared for analysis. Simultaneous optogenetic stimulation of cholinergic afferents with Pyr stimulation did not reveal an immediate enhancement of EPSP efficacy in synaptically coupled SST neurons for the first few pulses in the presynaptic spike train, inconsistent with a fast nAChR response at either pre- or postsynaptic locations (Supplemental Figure 1). Because PKA signaling had been implicated in enhancing transmission at Pyr to SST synapses, we hypothesized that the activation of signal transduction cascades might require some delay from nAChR activation to enhanced release (Cheng and Yakel, 2014, 2015a). Consistent with this, we observed a significant change in amplitude and failure rates ~200 ms after the onset of the light flash (Supplemental Figure 1), with a >3-fold increase in response amplitude (0.27±0.11 mV to 0.81±0.37 mV; n=4 and p=0.0002) and a nearly 2-fold reduction in mean failure rates (from 0.68±0.11 to 0.35±0.16, n=4 and p=0.03).

We thus examined the effect of ACh release on EPSP efficacy, using a 200 ms interval between the activation of cholinergic fibers and the stimulation of Pyr inputs. Remarkably, a single light pulse (10 ms) was sufficient to generate a significant increase in amplitude and a reduction in failure rates that nearly matched what had been observed with carbachol application (Figure 4; amplitude baseline 0.32±0.13 mV vs flash 0.62±0.15 mV; n=6 and p=0.04; failure rates baseline 0.58±0.09 vs flash 0.38±0.07; n=6 and p=0.0006).

To characterize the timecourse and duration of this cholinergic enhancement, we investigated two additional time intervals between the activation of cholinergic fibers and the stimulation of Pyr inputs, 50 ms and 500 ms (Supplemental Figure 2A,B). A 50 ms delay between optogenetically-released ACh and Pyr-SST synaptic activation did not change input strength, although it was sufficient to drive a significant reduction in failure rates. A 500 ms delay between ACh release and Pyr-SST synaptic activation did not alter either amplitude or failure rates. Finally we tested whether multiple flashes might augment the observed increase in Pyr-SST input strength. Increasing the number of flashes did not influence synaptic efficacy (Supplemental Figure 2C), likely due to pronounced synaptic depression at cholinergic terminals induced by prolonged optogenetic stimulation (data not shown).

To confirm that the ChAT-channelrhodopsin-mediated enhancement of Pyr-SST synaptic strength was acting through the same pathways as established using bath application of carbachol, we carried out the same experiments in the presence of the nAChR-antagonist mecamylamine. Similar to the effects described in Figure 3, pharmacological blockade of nAChRs prevented optogenetically-gated cholinergic enhancement of Pyr-SST connections

(Figure 4E,F; amplitude baseline 0.18±0.11 mV vs flash 0.20±0.10 mV; n=5 and p=0.99; failure rates baseline 0.72±0.09 vs flash 0.62±0.05; n=5 and p=0.38). Thus, we conclude that ACh release from endogenous cholinergic afferents acts through nAChRs to enhance local excitatory transmission onto neocortical SST neurons.

Timed, endogenous ACh release does not increase overall SST firing rates

Bath application of acetylcholine receptor agonists, using either ACh or the agonist carbachol, can induce a 3-fold increase in SST spontaneous firing activity (Chen et al., 2015a; Fanselow et al., 2008) (Figure 5A). This was not the case for Pyr neurons, where carbachol depolarized resting membrane potential (Supplemental Table 1) but was not sufficient to change Pyr spontaneous activity which was typically very low (<0.02 Hz). Consistent with other studies (Chen et al., 2015b; Fanselow et al., 2008), we found that mAChR but not nAChR activation was primarily responsible for the strong increase in spontaneous SST firing with carbachol.

Interestingly, brief optogenetically-activated release of ACh was not sufficient to influence overall firing rates of SST neurons in acute brain slices. A subset of SST neurons (4/18) could be driven to fire a single spike at short latency with a single light pulse (Figure 5B). However, the majority of SST neurons (14/18) responded to light-evoked ACh release with a brief depolarization followed by hyperpolarization (Figure 5B), suggestive of ACh-activated inhibition elsewhere in the local network (Alitto and Dan, 2013; Arroyo et al., 2012). . This delayed synaptic inhibition was eliminated in the presence of GABAa receptor antagonists (data not shown).

The difference in results for light-evoked ACh release versus the bath application of a cholinergic agonist underscores the importance of investigating neuromodulation delivered from endogenous sources: precisely-timed and highly local ACh release had specific effects that mapped onto only a subset of phenomenon observed with pharmacological treatments.

Basal forebrain afferents enhance Pyr-SST connections *in vivo*

Acute brain slices represent a useful platform for efficiently screening through drugs and conditions to characterize synaptic function. To determine whether precisely-timed cholinergic activation might also influence synaptic connections in intact circuits and compare the magnitude of these effects to acute brain slice analysis, we carried out paired whole-cell recordings between Pyr and SST neurons in somatosensory cortex of anaesthetized SST-Cre x Ai9 transgenic mice.

To examine how endogenous release of ACh affected Pyr-SST inputs *in vivo*, we virally transduced neurons in the basal forebrain of SST-Cre x Ai9 transgenic mice with a ChR2-expressing virus and then prepared animals for targeted whole-cell recordings 2–5 weeks later (Figure 6). Because basal forebrain afferents to the neocortex are almost exclusively cholinergic (Do et al., 2016), this ensured that acetylcholine was the primary neurotransmitter released. Indeed, we observed immunohistochemical colocalization of ChR2-expressing fibers with the vesicular acetylcholine transporter in superficial layers of S1 (Supplemental Figure 3).

We evaluated whether optogenetically-gated neurotransmitter release could influence EPSP amplitude *in vivo* using a single light pulse 200 ms prior to the test stimulus driving the presynaptic Pyr cell (Figure 6 and Supplemental Figure 4). Pyr and SST neurons were identified during the *in vivo* recording session and cell identity was confirmed using evoked firing output. Brief spike doublets were evoked in Pyr neurons and the EPSP amplitude of Pyr inputs in synaptically connected SST neurons were evaluated, where the EPSP triggered by the first spike of a doublet was compared before and after optogenetic activation of cholinergic afferents (see methods). Effects were remarkably similar to those observed in acute brain slices: a single light pulse significantly increased EPSP amplitude more than 2-fold (0.11±0.05 mV vs 0.31±0.06 mV; n=6; p=0.005) and reduced failure rates to 50.6±6% (vs 73.2±3.9% without stim; n=6; p=0.03). These results indicate that precisely-time activation of fibers from the basal forebrain can enhance the efficacy of Pyr to SST synapses in the intact brain.

To verify that the observed effects *in vivo* were due to the activation of nAChRs, we carried a subset of experiments where mecamylamine was included in the Ringer's solution above the brain and allowed to diffuse for at least 20 minutes before recording commenced. Under these conditions, optogenetic activation of basal forebrain afferents did not increase the amplitude of Pyr to SST connections, consistent with a cholinergic effect of stimulation (Figure 6I,J; amplitude baseline 0.23±0.07 mV vs flash 0.27±0.08 mV; p=0.38; failure rates baseline 0.65±0.04 vs flash 0.71±0.04; n=7 and p=0.17). Although ChR2 expression in the nucleus basalis and associated basal forebrain structures is not solely cholinergic, the mecamylamine-blockade of EPSP enhancement both *in vivo* and in acute brain slice indicates a common, nAChR-dependent mechanism.

Presynaptic nAChRs activate PKA signaling pathways to enhance release probability

Both anatomical and electrophysiological evidence indicate that nAChRs can be presynaptic in the mammalian cerebral cortex (Arroyo et al., 2012; Arroyo et al., 2014; Levy and Aoki, 2002; Lubin et al., 1999; McGehee et al., 1995; Vidal and Changeux, 1993), although some postsynaptic activity for these receptors has also been observed (Halff et al., 2014; Puddifoot et al., 2015). Because nAChR activation reduced the PPR and decreased failure rates, we hypothesized that these receptors were presynaptically localized.

We took advantage of the recording configuration afforded by direct analysis of synaptically coupled neuron pairs to determine whether nAChR-mediated PKA activation was required pre- or postsynaptically. To confirm that this increase was due to the activation of presynaptic pathways, we included the PKA inhibitor peptide PKI in the pipette internal solution for the presynaptic Pyr neuron, and experiments were carried out in acute brain slices where SST neurons had been virally labeled in a SST-Cre x ChAT-ChR2 transgenic mouse. Blocking PKA signaling in the presynaptic Pyr neuron was sufficient to prevent light-activated ACh release from enhancing synaptic efficacy at Pyr-SST connections (Figure 7 andSupplemental Figure 5; amplitude baseline 0.57±0.21 mV vs flash 0.47±0.17 mV; p=0.19; failure rates baseline 0.52±0.11 vs flash 0.55±0.11; n=8 and p=0.68). These results indicate that presynaptic nAChRs activate PKA signaling pathways to enhance synaptic strength at Pyr-SST synapses.

Pyr to PV synapses are not enhanced by endogenous ACh release

To assess whether the observed effects might facilitate input to other inhibitory neuron subtypes, we examined the effect of both pharmacological and optogenetic stimulation of cholinergic pathways on Pyr to PV neuron synapses (Figure 8). Although bath application of carbachol significantly increased EPSP amplitude (Supplemental Figure 6), unlike Pyr to SST connections, this effect was not recapitulated by optogenetic stimulation (amplitude baseline 1.55±0.59 mV vs flash 1.88±0.67 mV; p=0.18; failure rates baseline 0.17±0.06 vs flash 0.15±0.09; n=6 and p=0.82). Therefore, cholinergic enhancement of local excitatory input is target-specific, shifting the weight of excitatory drive toward SST but not PV neuron activation.

ACh does not influence synaptic strength at intracortical excitatory synapses

Our data indicate that precisely timed ACh release can influence local feedforward excitation onto SST neurons. To determine whether this was synapse-specific, we investigated the effect of optogenetically-evoked ACh release on direct synaptic connections between L2 Pyr neurons in a ChAT-ChR2 transgenic mouse (Figure 8). A single light flash 200 ms prior to the test train did not show any alteration in synaptic efficacy from Pyr inputs onto Pyr neurons (Figure 8 and Supplemental Figure 7).

To differentiate the effects of endogenous ACh release from prolonged drug application, we examined the effects of carbachol at Pyr-Pyr synapses (Supplemental Figure 7A, C). The net effect of carbachol on Pyr-Pyr connections in L2 was a modest but not significant synaptic depression, an effect that we hypothesized might be indirect, mediated by the mAChR-dependent increase in the firing activity of SST and other GABAergic neurons across the cortical network. Spontaneous SST firing is an important contributor to tonic, presynaptic GABAb activation that suppresses excitatory transmission in the neocortex (Urban-Ciecko et al., 2015). Consistent with this hypothesis, application of the GABAb antagonist CGP reversed this carbachol-induced synaptic depression between Pyr neurons, without showing any further enhancement of synaptic efficacy compared to baseline values (data not shown). As the mean amplitude of EPSPs was relatively large for the subset of the connections analyzed, it remains possible that endogenous ACh release might influence very small EPSPs between pyramidal neurons under some conditions.

These results indicate that the effects of endogenous ACh release on increasing excitatory drive are target-cell specific, enhancing local glutamatergic input to SST neurons without increasing recurrent excitation across the L2 network as a whole.

Discussion

It has long been known that excitatory inputs onto SST neurons are remarkably weak and strongly facilitating, even under optimized conditions (Beierlein et al., 2003; Fanselow et al., 2008; Levy et al., 2008; Pala and Petersen, 2015; Reyes et al., 1998). Prior studies have hypothesized that high-frequency firing is required to activate SST neurons (Berger et al., 2010; Kapfer et al., 2007; Silberberg and Markram, 2007); however, these regimes are not physiologically plausible for Pyr neurons in many areas of the neocortex, especially in

superficial layers where firing rates can be low (Barth and Poulet, 2012). Here we show that the weak synaptic efficacy of local excitatory inputs to SST neurons can be significantly and uniquely enhanced by spatially and temporally-specific ACh release. Remarkably, brief optogenetic activation of endogenous ACh release fully recapitulated the synaptic effects of bath-applied cholinergic agonists, without influencing resting membrane potential and mean spontaneous firing activity of SST neurons observed with drug application.

Functional versus anatomical connectivity in neocortical networks

Anatomical mapping of cell-type specific synaptic connections across the cortical column has been an important goal of many recent investigations, using both serial blockface EM reconstruction and rabies-virus approaches to provide quantitative detail about circuit function (see for example (Bock et al., 2011; Wall et al., 2016). The weak functional contribution of Pyr-SST connections are at odds with their ubiquitous anatomical presence and underscore the importance of electrophysiological analysis to infer circuit processing capabilities. Our results show that state-dependent synaptic modulation can effectively rewire cortical circuits, shifting the balance of inhibition by engaging SST neurons with local input when acetylcholine levels are transiently increased. On face, the fast circuit rewiring observed here is conceptually similar to previous studies showing that GABAb signaling can silence recurrent excitatory connections in the L2 network (Urban-Ciecko et al., 2015). Defining the dynamic range for synaptic function is required for proper estimation of how specific synaptic motifs are recruited during different brain states and neuromodulatory conditions.

Molecular properties of Pyr-SST synapses

The weak and strongly facilitating properties of Pyr-SST synapses have been well-established. Prior studies in acute brain slices have significantly overestimated synaptic strength due to elevated extracellular Ca^{2+} and the absence of network activity that may suppress inputs (Borst, 2010; Urban-Ciecko et al., 2015). Importantly, this overestimation has required correction in simulations (Markram et al., 2015). What are the molecular mechanisms that regulate transmission at Pyr to SST synapses? Low release probability at excitatory inputs to SST neurons may be linked to postsynaptic expression of Elfn1 (Sylwestrak and Ghosh, 2012), expressed in the hippocampus and a sparse subset of neocortical neurons. Activation of presynaptic metabotropic (Tomioka et al., 2014) and calcium-permeable kainate receptors (Sun et al., 2009) can increase EPSP amplitude in SST neurons in the hippocampus; however, the source of glutamate for activation of these presynaptic receptors is likely to be from the terminal itself, and becomes apparent only at later spikes in a train. Prior molecular studies have not revealed scenarios by which Pyr input to SST neurons can be engaged in the absence of prolonged high-frequency firing.

Instead, we hypothesized that there may be additional pathways by which Pyr-SST connections could be augmented. The nAChR-dependent facilitation of Pyr-SST inputs meet criterion for a pathway that could effectively enhanced activation of this synaptic motif at physiologically-relevant Pyr cell firing rates. We predict that brain states characterized by increases in ACh activity and the synchronized activation of cholinergic fibers during cue-

related reward or punishment (Hangya et al., 2015) will be associated with effective engagement of disynaptic inhibition through this common synaptic motif.

Our studies did not reveal the subtype of nAChRs that are responsible for Pyr to SST synaptic enhancement. Prior studies provide evidence for both alpha 7 as well as alpha 4, beta 2 subunits in mouse neocortical tissue (Atlas; McGehee et al., 1995). Although atropine – which did not block the synaptic effects described here-can also antagonize alpha 4, beta 2 subunit-containing receptors (Parker et al., 2003) and might suggest alpha 7-containing receptors, the slow timecourse of the effect is consistent with a role for non-alpha 7 containing receptors (Arroyo et al., 2012). Future studies with a comprehensive pharmacological analysis will help reveal the specific nAChR subtypes involved in these effects.

Functional consequences of ACh release timing on cortical processing

Pharmacological studies with persistent cholinergic application over many minutes have provided abundant evidence for cholinergic signaling in neocortical circuits, where effects have been attributed both to muscarinic and nicotinic receptors. Recent studies using temporally precise optogenetic stimulation of cholinergic afferents (Alitto and Dan, 2013; Chen et al., 2015b; Hangya et al., 2015; Joshi et al., 2016) have refined the hypotheses about how the effects of endogenous ACh release compares to prior pharmacological studies, where AChR activation can be prolonged and direct and indirect effects can be difficult to disentangle.

Prior studies have not been able to reveal whether the temporal and spatial organization of cholinergic release can activate different receptor subtypes, in different cellular compartments and across different neuronal subtypes. In addition, efforts to investigate how endogenous ACh release functions have typically employed non-physiological, high-frequency stimulation of afferents (Chen et al., 2015b; Joshi et al., 2016; Kuchibhotla et al., 2017) that do not represent normal regimes of ACh fiber activation. Here we show that brief and precisely-timed optogenetic activation of ACh release mimics the synaptic, nAChR-dependent effects of cholinergic agonists without recapitulating the profound changes in network activity that may be due to the activation of mAChRs. The ability to dissociate synaptic and network effects with precise optical stimulation suggests that there may be multiple conditions for subtype-specific ACh-signaling depending on the task at hand. It is tempting to speculate that cholinergic neurons of the basal forebrain take advantage of these different regimes to achieve different network functions.

nAChRs, cognitive disorders, and sensory processing

Acetylcholine signaling and the activity of cholinergic neurons in the basal forebrain are biochemical correlates of attention and cue salience (Picciotto et al., 2012), and cholinergic activity has been linked to both muscarinic and nicotinic AChR activation (see for example muscarinic (Herrero et al., 2008) and nicotinic (Guillem et al., 2011). Nicotinic AChRs in particular have been linked to sensory processing deficits in schizophrenia and attention disorders (Freedman, 2014; Guillem et al., 2011; Parikh et al., 2016). Our findings suggest that selective engagement of feedback inhibition through SST neurons might be essential for

enhanced sensory processing in the attentive, cued state. The high failure rate of Pyr to SST inputs suggests that local drive to SST neurons is negligible under normal conditions when Pyr cell firing rates are low. However, during active sensation, cholinergic enhancement of local input may be amplified by the sheer number of firing pyramidal neurons with convergent input onto SST neurons. Under these conditions, strong feedback inhibition through SST neurons is likely to occur, effects that selectively enhance short-latency evoked responses and reduce recurrent network activity.

The asynchronous state and synapse-specific cholinergic enhancement of EPSP efficacy

ACh neurons increase their firing rates during movement or arousal in awake rodents and have been linked to a global increase in cortical activity (Buzsaki et al., 1988; Eggermann et al., 2014; Metherate et al., 1992) and a decrease in correlated firing of neurons in the neocortex of primates as well as rodents (Cohen and Maunsell, 2009; Herrero et al., 2008; Pafundo et al., 2016; Renart et al., 2010).

The synapse-selective effects of ACh on enhancing excitatory drive onto a subtype of inhibitory neurons without influencing feedforward excitatory connections (Pyr-Pyr connections) is consistent with a link between increased inhibition and the desynchronized state (Doiron et al., 2016). The desynchronous cortical state has been associated with attention, enhanced sensory processing, and increased activity of cholinergic neurons in the basal forebrain (Castro-Alamancos, 2004; Cohen and Maunsell, 2009; Marguet and Harris, 2011; Poulet and Petersen, 2008).

The synapse-selective nAChR-mediated effects identified here are predicted to enhance inhibition without altering excitation, and suggest a potential link between the selective engagement of SST-mediated inhibition, network desynchronization and the behavioral correlates of attention. Transient cholinergic activity may enable the cortical network to engage alternative processing strategies depending upon brain state, a design structure that has parallels in such as field-programmable gate arrays, an integrated circuits in computer chips, where hardware can be dynamically reconfigured according to user demands.

It is tantalizing to imagine that the cholinergic enhancement of SST-mediated feedback inhibition may be linked to specific alterations in cognitive function in awake and behaving animals. Towards these ends, future experiments to determine how specific microcircuits perform during different brain states and behavioral demands will be critical.

Experimental model and subject details

Animals

All experiments in acute brain slices were conducted in accordance with the National Institute of Health guidelines and were approved by the Institutional Animal Care and Use at Carnegie Mellon University. *In vivo* recording experiments performed in Germany were carried out in accordance with national and local Animal Welfare Office regulations.

Wild-type C57Bl6 mice and transgenic mice from Jackson Labs were used. The following strains of transgenic mice were used 1) SST-IRES-Cre mice on a mixed background,

C57Bl6J and B6;129S6 (stock # 013044); 2) Ai14 and Ai9 mice on a mixed background, C57Bl6J and B6;129S6 (#007908) and (#007909), respectively; 3) Ai3 on a C57Bl6 background (# 007903); 4) ChAT-ChR-YFP-BAC on a C57Bl6 background (#014545); 5) PValb-2A-Cre on a C57Bl6 background (#013044). Animals were used irrespective of sex, and both males and females were employed.

Experiments were performed in offspring of SST-IRES-Cre mice crossed to either Ai14 or Ai9 (floxed-Tdt) or Ai3 (floxed-YFFP) reporter mice, in ChaT-ChR2-YFP-BAC mice crossed to SST-IRES-Cre mice or to C57/Bl6 (Jackson Lab), in offspring of PValb-2A-Cre mice crossed to either Ai14 or Ai9 reporter mice, in ChaT-ChR2-YFP-BAC mice crossed to PValb-2A-Cre mice. All transgenes were used as heterozygotes.

Method details

Virus injection

For acute brain slice recordings, in double transgenic mice (SST-IRES-Cre-ChaT-ChR2 or PValb-2A-Cre-ChaT-ChR2) a flex–mCherry or-TdTomato virus was injected to the barrel cortex to visualize SST neurons or PV neurons, respectively. Mice, aged between postnatal days 10–15, were anesthetized with 2.0% – 2.5% isoflurane and immobilized in a stereotaxic frame. A small craniotomy was made over the barrel cortex, typically 0.75 mm posterior to Bregma and 3.0 mm lateral to the midline. A 33-gauge, stainless steel cannula (PlasticsOne C315I/SPC, ~0.2 mm) was then inserted 0.5 mm below the pia, and held for 5 min to allow for the tissue to regain a convex shape. Using an attached syringe pump (Stoelting 78–0210S), 0.4 μL of 1.25×10^{13} GC/mL AAV9, carrying a floxed Tdt gene under a CAG promoter (Penn Vector Core AV-9-ALL864, lot CS0634) was then delivered at a rate of 0.08 μL/min. The virus was then allowed to spread for 10 min before cannula withdrawal. Experiments were conducted 5–10 days after virus injection.

For *in vivo* recordings, P9 to P13 double transgenic mice (SST-IRES-cre-Ai9) were anesthetized with *i.p.* injection of ketamine (100 mg/kg) and xylaxine (5 mg/kg) and infected with an AAV9/2 CamKII-ChR2(T159C)-p2A-EYFP (Berndt et al., 2011) or VSVG.HIV.SIN.Synapsin.ChR2 (H134R).EYFP.WP (Addgene 20945) (Berndt et al., 2011) (Charité Vector Core) virus in the substantia innominata and associated basal forebrain structures (Bregma: 0.02 mm, lat: 1.3 mm, depth: 4.5 mm) . Briefly, a small craniotomy was made to allow a 10 – 20 μm tip diameter glass pipette to be lowered to the injection site. Virus was injected using a Narishige oil piston (MO-10, Narishige) at a rate of 50 nl/min for a total volume of 600 nl. After injection the glass pipette was maintain in place for 5 min before being retracted. Recordings were performed 2–4 weeks after virus injection.

Brain slice preparation

Experiments were done in mice aged P18–P23, where P0 indicates the day of birth. Brain slices (350 μm thick) were prepared by an “across-row” procedure in which the anterior end of the brain was cut along a 45° plane toward the midline (Finnerty et al., 1999). Slices were cut, recovered and maintained at room temperature (24°C) in artificial cerebrospinal fluid

(ACSF) composed of (in mM): 119 NaCl, 2.5 KCl, 2 $MgSO_4$, 2 CaCl2, 1 NaH_2PO_4, 26.2 $NaHCO_3$, 11 glucose equilibrated with 95/5% O_2/CO_2.

Whole-cell recording in acute brain slices

Whole-cell recording was performed from somata of layer 2/3 (L2/3) neurons in primary somatosensory (barrel) cortex using borosilicate glass electrodes, resistance 4–8 MΩ. For EPSP recording, electrode internal solution was composed of (in mM): 125 potassium gluconate, 2 KCl, 10 HEPES, 0.5 EGTA, 4 MgATP, and 0.3 NaGTP, at pH 7.25–7.35, 290 mOsm.

Internal solutions contained trace amounts of Alexa 568 or 488 to verify the neuronal types and the location of the recorded cell. Because of the difficulty in identifying connected pairs, the majority of recordings were carried out at room temperature (24°C) to enable longer recording periods, since prolonged incubation at warmer temperatures degrades cell health and recording quality. A subset of recordings were carried out at 32–35°C; no differences in synaptic efficacy were observed under these conditions.

Whole-cell recording *in vivo*

P18-P38 mice were anesthetized with 1.5–2% isoflurane and maintain at 37°C during the surgery. A small craniotomy (~1mm diameter) was made over the somatosensory cortex and the dura removed under Ringer's solution (in mM): 135 NaCl, 5 KCl, 5 HEPES, 1.8 $CaCl_2$, 1 $MgCl_2$. Mice were injected *i.p.* with 1.5 mg/kg of urethane and transferred to a Femto2D *in vivo* 2-photon laser-scanning microscope (Femtonics). SST neurons expressing the fluorophore TdTomato were visualized at 950 nm while Alexa 594 used to identified cell bodies, were visualized at 820 nm using a Chameleon Ultra II (Coherent) pulsed laser light source (Jouhanneau et al 2015). Targeted whole cell patch clamp recording were made with 2 mm borosilicate glass electrodes (Hilgenberg) with a resistance of 5–7 MΩ. Recording pipettes were filled with intracellular solution containing, in mM: 135 potassium gluconate, 4 KCl, 10 HEPES, 10 phosphocreatine, 4 MgATP, 0.3 NaGTP (adjusted to pH 7.3 with KOH), 2 mg/ml biocytin with 25 μM Alexa 594 added immediately prior to recording. Two to three recording pipettes were inserted into the brain. High positive pressure (180 mBar) was used to penetrate the brain surface then instantly reduce to 60 mBar to lower the pipette to approximately 100 μm under the pia. Then the pressure was further reduced to 30 mBar to finally approach the targeted cells. The contact with the neuron was detected using an oscilloscope (Tektronix TDS2024C) as well as visualized on the screen during 2-photon scanning imaging. When the contact was confirmed the positive pressure was released and a slight negative pressure was applied to achieve a gigaseal. After membrane break-in, neurons were maintained under current clamp mode. Recordings were made using an Axon MultiClamp 700B amplifier (Molecular Devices) with an Ag/AgCl ground electrode in the recording chamber. Recordings were filtered at 10 kHz and digitized at 20 kHz via an ITC18 (Heka) analogue-to-digital converter connected to a PC under the control custom software for IgorPro (Wavemetrics).

Neuron classification

Brain slice: Cells were classified as pyramidal neurons according to pyramidal-like soma shape, the presence of an apical dendrite and spines visible after Alexa filling reconstruction as well as according to regular spiking responses to 500 ms suprathreshold intracellular current injection. Inhibitory neurons were identified using fluorescent reporter gene expression. Additionally, characteristic firing responses to further validate cell identity were collected.

The majority of SST neurons are low-threshold spiking (LTS); however, about 10% of SST neurons are fast spiking (FS) (Hu et al., 2013; Urban-Ciecko et al., 2015). LTS firing using square pulse current injections demonstrated spike-rate adaptation, and the AHP after the first action potential was more negative than the last AHP during the current step. FS cells were identified by a non-adapting firing patterns and AHP magnitudes that were uniform throughout a given current step. Only LTS SST neurons were included for further analysis. Pyr inputs to fluorescently-labeled FS, SST-Cre+ neurons showed low failure rates and exhibited synaptic depression. This synaptic phenotype was similar to Pyr inputs to fluorescently-labeled FS, PV-Cre+ neurons. All PV neurons were verified to be FS.

In vivo: Input resistance and firing patterns of all recorded neurons were determined using square pulse current injections with different amplitudes. To reveal the firing pattern of the targeted cell, 500 ms current pulses −200, −100, 0, 100, 200, 300 pA were used. Input resistance was assessed using square current pulses −100 pA of 200 ms duration. SST inhibitory neurons were identified by their reporter gene expression tdT visualized under 950 nm wavelength. Pyr cell identity was further confirmed using live 2-photon fluorescent images made directly after the end of the recording session, when apical dendrite and spines are visible (Jouhanneau et al, 2015).

Connectivity analysis

Brain slice: Synaptically connected cells were identified by paired whole-cell patch-clamp recordings, where pyramidal cells were targeted based on morphology and SST neurons were targeted based on fluorescent markers in transgenic mice. The distance between cells was no longer than 200 μm. The distance from the pia was typically between 200–250 μm. Recordings were performed in 2 ACSF solutions that differed only by concentrations of Mg^{2+}, Ca^{2+}, and K+. Ionic concentrations were as follows (in mM): physiological Ca^{2+} −1 $CaCl_2$, 0.5 $MgSO_4$, 3.5 KCl or elevated Ca^{2+} −2.5 $CaCl_2$, 1.3 $MgSO_4$, 2.5 KCl. A series of 10 pulses (0.8–1 nA, 3–5 ms duration) at 20 Hz were delivered across 20 separate trials (0.1 Hz) to a cell assigned as the trigger (presynaptic) cell.

Because SST neurons are spontaneously active in mACSF, EPSP properties evoked in SST neurons were evaluated at the hyperpolarized membrane potential below the spike threshold (−60 mV, typically). Pyramidal cells were maintained at their normal resting potential, i.e., current was not injected to maintain a specific resting membrane potential during the course of the experiment.

Since recurrent activity in network, Upstates made evoked synaptic responses identification difficult, only responses collected during Downstates were evaluated. In cells where activity

was compared across different recording solutions, mACSF and rACSF were applied in random order. V*rest* was adjusted in SST neurons for the same value in different solutions when EPSPs were collected. Spontaneous firing frequency was analyzed by counting action potentials over 4–5 minutes of recording in different ACSFs and V*rest* was not corrected.

Electrophysiological data were acquired by Multiclamp 700A (Molecular Devices) and a National Instruments acquisition interface. The data were filtered at 3 kHz, digitized at 10 kHz and collected by Igor Pro 6.0 (Wavemetrics). Input resistance and Access resistance were analyzed online. Depolarization-induced suppression of excitation was tested by stimulating SST neuron with a train of 10 pulses (0.8–1 nA, 3–5 ms duration) at 10Hz delivered 5 sec before the pyramidal cell stimulation with the series of 10 pulses at 20Hz. The protocol was repeated 10 times every 90 sec. Naturalistic stimulation (Figure 1B) was set according to a spike train obtained in the somatosensory cortex of the front paw of a mouse during forepaw movement (unpublished data). The stimulus set consisted of 5 pulses (0.8–1 nA, 3–5 ms duration) at the following times (sec): 0, 0.016, 0.036, 3.707, 6.012. The protocol was repeated 25 times.

For *in vivo* experiments, connectivity between Pyr neurons and SST interneurons was initially assessed under dual whole-cell current clamp recording configuration using trains of 5–10 spikes elicited in the Pyr neurons by depolarizing it for 500 ms during the first 1–2 minutes of recording.

Optical stimulation

Acute brain slices: For ChR2 activation, photo stimulation was produced by a light-emitting diode (white LED with appropriate fluorescence filters 535 nm and 480 nm, respectively). The stimulation intensity was set to maximum range (Prizmatix, Israel) and delivered through a 40x water-immersion objective.

Cholinergic fibers were activated by single pulses (10 ms) delivered at different times related to pyramidal cell activation: either, at same time as Pyr neuron stimulation (0 delay), or 1 single light pulse at −50 ms, −200 ms, or −500 ms before Pyr neuron stimulation, or with a train of 20 photo pulses at 12.5 Hz before Pyr neuron stimulation. Trials were delivered at 0.1 Hz, and at least 20 baseline (light-OFF) trials were collected before initiating light-ON trials.

In vivo: The experiment consisted in two trials of 1 min each: one without optogenetic activation of Ach fibers (OFF trial) and one with optogenetic activation of Ach fibers (ON trial). Doublets of action potentials (APs) were elicited by injecting (20–50 ms) current pulses into the Pyr neurons at 1Hz. During the ON trial Ach fibers expressing ChR2 were stimulated with a 10 ms single pulse of LED blue light (475 nm) placed 5 – 15 mm away from the recording location, 200 ms before the Pyr neuron stimulation.

Pharmacology

The following agents were used for bath-application in acute brain slice experiments: forskolin, cell-permeable activator of adenylyl cyclase (50 μM, Tocris), selective cAMP-specific phosphodiesterase (PDE4) inhibitor rolipram (0.1 μM, Sigma), the noradrenergic

agonist norepinephrine (50 μM, Sigma), the serotonin receptor agonist serotonin (10 μM, Tocris), the dopamine receptor agonist CY 208–243 (50 μM, Tocris), P2 receptor agonist adenosine (100 μM, Sigma), the CB1 receptor antagonist AM 251 (1 μM, Tocris), the group I metabotropic glutamate receptor agonist DHPG (10 μM, Sigma). Cholinergic drugs used were the agonist carbachol (20 μM, Sigma), the nicotinic acetylcholine receptor antagonist mecamylamine (*in vitro*; 10 μM, Sigma), the muscarinic receptor antagonist atropine (10 μM, Sigma). We note that at the concentrations used, atropine may modestly block a subset of nAChRs that contain the alpha 4 beta 2 subunits (Parker et al., 2003). PKA inhibitor fragment PKI (100 nM, Tocris) was diluted in the internal solution and data were collected 15 minutes after the break-in the membrane. Other pharmacological agents were bath applied for at least 10 minutes before assessing EPSP properties. Stimuli were not delivered during drug wash-on.

To assess the role of the nAChRs in modulating Pyr to SST synapses *in vivo*, the antagonist mecamylamine was used at a concentration 500 μM (Sigma) applied directly in the recording chamber for at least 20 min before to start the experiments.

Immunohistochemistry

After the recording session, mice were injected *i.p.* with an additional dose of urethane (1.5 mg/kg) and transcardially perfused with cold 0.1 M PBS followed by 4% PFA. Brains were removed and postfixed overnight at 4°C in 4 % PFA. Coronal slices (100 μm) were performed using a vibratome (Leica VT1000S). Sections were washed in 0.1 M PBS and permeabilized in Triton/PBS (0.3% vol/vol). Sections were then incubated 2 hours in a blocking solution (5% goat serum in 0.3%bTriton/PBS). Section were then incubated overnight at 4°C in primary antibodies against: GFP (chicken anti-GFP, 1:250 in 0.3 % Triton/PBS, Abcam: ab13970) and VAChT (rabbit anti-VAChT, 1:250 in 0.3 % Triton/PBS, Synaptic system: Sysy 139103). Sections were washed then incubated overnight at 4°C in fluorescent conjugated secondaries (488-conjugated goat anti-chicken IgG 1:250 in 0.3 % Triton/PBS, ThermoFisher: A11039; and 647-conjugated goat anti-rabbit IgG 1:250 in 0.3 % Triton/PBS, respectively). Section were washed and mounted onto glass slides using DAPI fluoromount-G (SouthernBiotech, 0100–20) and visualized using a Zeiss upright microscope. Images were acquired using the ZEN software (Zeiss). All images were imported and analyzed using the ImageJ plugin Fiji v1.0.

Quantification and statistical analysis

For acute brain slice recording

In every condition, evoked EPSPs were analyzed from 10 trials of 10-pulse trains. Measurements of amplitude and failure rates are plotted for the EPSP evoked by the first artificial pulse only. All plotted amplitude measurements include response failures; that is, trials where there was no detectable EPSP. The minimal detectable amplitude was 0.019 mV. A failure was considered as a response below ~1 standard deviation of the noise. We considered responses to the first presynaptic spike to be most representative of synaptic function occurring *in vivo*, because L2/3 pyramidal neurons rarely fire more than a single spike and almost never at frequencies exceeding 20 Hz *in vivo.*

For heat-map figures, amplitudes for all EPSPs are shown. For all heat-map figures of EPSP responses across the entire 10-pulse train, maximum amplitude (red) was set for the individual connection plotted. Because, very often a single presynaptic action potential in a pyramidal neuron does not evoke EPSP in SST neuron, normalization was applied to compare the amplitude (or failure rates) during 2 different conditions e.g. to compare light ON and light OFF trials or pre and post drug applications. Normalization was set by adding the value 1 to both pre-and post- values.

Population data are presented as mean ± SEM, n represents number of cells that is typically equal to the number of animals. Statistical significance was defined as $p<0.05$ using a two-tailed unequal variance t-test. When two conditions were compared within the same cell a two-tailed paired t-test was used (parametric or non-parametric (Wilcoxon)). Gaussian distribution was tested with the method of Kolmogorov and Smirnov using GraphPad InStat (demo) program.

For *in vivo* recording

Only Downstate membrane potential responses in SST neurons were averaged (n=7 to 47 trials). EPSP amplitude was defined as the peak membrane potential (Vm) response between 2 – 10 ms after the presynaptic pyramidal AP. The amplitude was calculated by subtracting 1ms average baseline Vm before the presynaptic AP to the 1 ms average Vm at the peak of the EPSP. We compared the averaged amplitude of the 1st EPSP during light OFF trial to the 1st EPSP averaged amplitude in light ON trial. Failure was considered as a response below ~1.5 standard deviation of the noise. Failure rates were calculated as the number of failures divided by the number of presynaptic spikes. Population data are presented as mean ± SEM. Statistical significance was calculated based on the non-parametric two-tailed paired Wilcoxon sign rank test using Igor Pro 6 (Wavemetrics). For histological assessment of ChR2-expression in the basal forebrain, mice were perfused with 4 % PFA after recording and brains removed, post-fixed overnight in 4% PFA, and then sectioned for post-hoc histological analysis and confirmation of injection site.

Supplementary Material

Refer to Web version on PubMed Central for supplementary material.

Acknowledgements

Special thanks to Joanne Steinmiller for expert animal care, and Megumi Matsushita and Rogan Grant for technical assistance. We would like to thank Janett König and Charlene Memler for technical assistance and Dr. Phillip Wisinski-Bokiniec for his imaging technical support. This work was supported by the McKnight Foundation (ALB) and NIH R01NS088958 (ALB and JFAP), the National Science Centre, Poland (2015/18/E/NZ4/00721; JUC), the European Research council (ERC-2015-CoG-682422; JFAP), the DFG (DFG-FOR-2143-Interneuron; JFAP), the Berlin Institute of Health (BIH; JFAP) and the European Union (FP7, 3×3Dimaging 323945; JFAP).

References

Alitto HJ, and Dan Y (2012). Cell-type-specific modulation of neocortical activity by basal forebrain input. Front Syst Neurosci 6, 79. [PubMed: 23316142]

Alitto HJ, and Dan Y (2013). Cell-type-specific modulation of neocortical activity by basal forebrain input. Front Syst Neurosci 6, 79. [PubMed: 23316142]

Anwyl R (1999). Metabotropic glutamate receptors: electrophysiological properties and role in plasticity. Brain Res Brain Res Rev 29, 83–120. [PubMed: 9974152]

Arroyo S, Bennett C, Aziz D, Brown SP, and Hestrin S (2012). Prolonged disynaptic inhibition in the cortex mediated by slow, non-alpha7 nicotinic excitation of a specific subset of cortical interneurons. The Journal of neuroscience : the official journal of the Society for Neuroscience 32, 3859–3864. [PubMed: 22423106]

Arroyo S, Bennett C, and Hestrin S (2014). Nicotinic modulation of cortical circuits. Front Neural Circuits 8, 30. [PubMed: 24734005]

Atlas, AB; http://mouse.brain-map.org.

Auerbach A, and Akk G (1998). Desensitization of mouse nicotinic acetylcholine receptor channels. A two-gate mechanism. J Gen Physiol 112, 181–197. [PubMed: 9689026]

Barth AL, and Poulet JF (2012). Experimental evidence for sparse firing in the neocortex. Trends Neurosci 35, 345–355. [PubMed: 22579264]

Beierlein M, Gibson JR, and Connors BW (2003). Two dynamically distinct inhibitory networks in layer 4 of the neocortex. Journal of neurophysiology 90, 2987–3000. [PubMed: 12815025]

Berger TK, Silberberg G, Perin R, and Markram H (2010). Brief bursts self-inhibit and correlate the pyramidal network. PLoS Biol 8.

Berndt A, Schoenenberger P, Mattis J, Tye KM, Deisseroth K, Hegemann P, and Oertner TG (2011). High-efficiency channelrhodopsins for fast neuronal stimulation at low light levels. Proceedings of the National Academy of Sciences of the United States of America 108, 7595–7600. [PubMed: 21504945]

Bock DD, Lee WC, Kerlin AM, Andermann ML, Hood G, Wetzel AW, Yurgenson S, Soucy ER, Kim HS, and Reid RC (2011). Network anatomy and in vivo physiology of visual cortical neurons. Nature 471, 177–182. [PubMed: 21390124]

Borst JG (2010). The low synaptic release probability in vivo. Trends Neurosci 33, 259–266. [PubMed: 20371122]

Buzsaki G, Bickford RG, Ponomareff G, Thal LJ, Mandel R, and Gage FH (1988). Nucleus basalis and thalamic control of neocortical activity in the freely moving rat. The Journal of neuroscience : the official journal of the Society for Neuroscience 8, 4007–4026. [PubMed: 3183710]

Cachelin AB, and Colquhoun D (1989). Desensitization of the acetylcholine receptor of frog end-plates measured in a Vaseline-gap voltage clamp. The Journal of physiology 415, 159–188. [PubMed: 2561785]

Castro-Alamancos MA (2004). Absence of rapid sensory adaptation in neocortex during information processing states. Neuron 41, 455–464. [PubMed: 14766183]

Chavis P, Nooney JM, Bockaert J, Fagni L, Feltz A, and Bossu JL (1995). Facilitatory coupling between a glutamate metabotropic receptor and dihydropyridine-sensitive calcium channels in cultured cerebellar granule cells. The Journal of neuroscience : the official journal of the Society for Neuroscience 15, 135–143.

Chen N, Sugihara H, and Sur M (2015a). An acetylcholine-activated microcircuit drives temporal dynamics of cortical activity. Nature neuroscience 18, 892–902. [PubMed: 25915477]

Chen N, Sugihara H, and Sur M (2015b). An acetylcholine-activated microcircuit drives temporal dynamics of cortical activity. Nat Neurosci 18, 892–902. [PubMed: 25915477]

Cheng Q, and Yakel JL (2014). Presynaptic alpha7 nicotinic acetylcholine receptors enhance hippocampal mossy fiber glutamatergic transmission via PKA activation. The Journal of neuroscience : the official journal of the Society for Neuroscience 34, 124–133.

Cheng Q, and Yakel JL (2015a). Activation of alpha7 nicotinic acetylcholine receptors increases intracellular cAMP levels via activation of AC1 in hippocampal neurons. Neuropharmacology 95, 405–414. [PubMed: 25937212]

Cheng Q, and Yakel JL (2015b). The effect of alpha7 nicotinic receptor activation on glutamatergic transmission in the hippocampus. Biochem Pharmacol 97, 439–444. [PubMed: 26212541]

Cochilla AJ, and Alford S (1998). Metabotropic glutamate receptor-mediated control of neurotransmitter release. Neuron 20, 1007–1016. [PubMed: 9620704]

Cohen MR, and Maunsell JH (2009). Attention improves performance primarily by reducing interneuronal correlations. Nature neuroscience 12, 1594–1600. [PubMed: 19915566]

Dawson LA, Nguyen HQ, and Li P (2001). The 5-HT(6) receptor antagonist SB-271046 selectively enhances excitatory neurotransmission in the rat frontal cortex and hippocampus. Neuropsychopharmacology 25, 662–668. [PubMed: 11682249]

Do JP, Xu M, Lee SH, Chang WC, Zhang S, Chung S, Yung TJ, Fan JL, Miyamichi K, Luo L, et al. (2016). Cell type-specific long-range connections of basal forebrain circuit. Elife 5.

Doiron B, Litwin-Kumar A, Rosenbaum R, Ocker GK, and Josic K (2016). The mechanics of state-dependent neural correlations. Nature neuroscience 19, 383–393. [PubMed: 26906505]

Eggermann E, Kremer Y, Crochet S, and Petersen CC (2014). Cholinergic signals in mouse barrel cortex during active whisker sensing. Cell Rep 9, 1654–1660. [PubMed: 25482555]

Fanselow EE, Richardson KA, and Connors BW (2008). Selective, state-dependent activation of somatostatin-expressing inhibitory interneurons in mouse neocortex. J Neurophysiol 100, 2640–2652. [PubMed: 18799598]

Finnerty GT, Roberts LS, and Connors BW (1999). Sensory experience modifies the short-term dynamics of neocortical synapses. Nature 400, 367–371. [PubMed: 10432115]

Freedman R (2014). alpha7-nicotinic acetylcholine receptor agonists for cognitive enhancement in schizophrenia. Annu Rev Med 65, 245–261. [PubMed: 24111888]

Garcia-Junco-Clemente P, Ikrar T, Tring E, Xu X, Ringach DL, and Trachtenberg JT (2017). An inhibitory pull-push circuit in frontal cortex. Nature neuroscience.

Gentet LJ, Kremer Y, Taniguchi H, Huang ZJ, Staiger JF, and Petersen CC (2012). Unique functional properties of somatostatin-expressing GABAergic neurons in mouse barrel cortex. Nat Neurosci 15, 607–612. [PubMed: 22366760]

Gil Z, Connors BW, and Amitai Y (1997). Differential regulation of neocortical synapses by neuromodulators and activity. Neuron 19, 679–686. [PubMed: 9331357]

Gioanni Y, Rougeot C, Clarke PB, Lepouse C, Thierry AM, and Vidal C (1999). Nicotinic receptors in the rat prefrontal cortex: increase in glutamate release and facilitation of mediodorsal thalamo-cortical transmission. Eur J Neurosci 11, 18–30. [PubMed: 9987008]

Guillem K, Bloem B, Poorthuis RB, Loos M, Smit AB, Maskos U, Spijker S, and Mansvelder HD (2011). Nicotinic acetylcholine receptor beta2 subunits in the medial prefrontal cortex control attention Science (New York, NY 333, 888–891. [PubMed: 21836018]

Halff AW, Gomez-Varela D, John D, and Berg DK (2014). A novel mechanism for nicotinic potentiation of glutamatergic synapses. The Journal of neuroscience : the official journal of the Society for Neuroscience 34, 2051–2064.

Hangya B, Ranade SP, Lorenc M, and Kepecs A (2015). Central Cholinergic Neurons Are Rapidly Recruited by Reinforcement Feedback. Cell 162, 1155–1168. [PubMed: 26317475]

Hassani OK, Lee MG, Henny P, and Jones BE (2009). Discharge profiles of identified GABAergic in comparison to cholinergic and putative glutamatergic basal forebrain neurons across the sleep-wake cycle. The Journal of neuroscience : the official journal of the Society for Neuroscience 29, 11828–11840.

Herrero JL, Roberts MJ, Delicato LS, Gieselmann MA, Dayan P, and Thiele A (2008). Acetylcholine contributes through muscarinic receptors to attentional modulation in V1. Nature 454, 1110–1114. [PubMed: 18633352]

Hilscher MM, Leao RN, Edwards SJ, Leao KE, and Kullander K (2017). Chrna2-Martinotti Cells Synchronize Layer 5 Type A Pyramidal Cells via Rebound Excitation. PLoS Biol 15, e2001392. [PubMed: 28182735]

Hu H, Cavendish JZ, and Agmon A (2013). Not all that glitters is gold: off-target recombination in the somatostatin-IRES-Cre mouse line labels a subset of fast-spiking interneurons. Front Neural Circuits 7, 195. [PubMed: 24339803]

Jiang X, Shen S, Cadwell CR, Berens P, Sinz F, Ecker AS, Patel S, and Tolias AS (2015). Principles of connectivity among morphologically defined cell types in adult neocortex Science (New York, NY 350, aac9462. [PubMed: 26612957]

Joshi A, Kalappa BI, Anderson CT, and Tzounopoulos T (2016). Cell-Specific Cholinergic Modulation of Excitability of Layer 5B Principal Neurons in Mouse Auditory Cortex. The Journal of neuroscience : the official journal of the Society for Neuroscience 36, 8487–8499.

Kano M, Ohno-Shosaku T, Hashimotodani Y, Uchigashima M, and Watanabe M (2009). Endocannabinoid-mediated control of synaptic transmission. Physiol Rev 89, 309–380. [PubMed: 19126760]

Kapfer C, Glickfeld LL, Atallah BV, and Scanziani M (2007). Supralinear increase of recurrent inhibition during sparse activity in the somatosensory cortex. Nat Neurosci 10, 743–753. [PubMed: 17515899]

Kawaguchi Y, and Shindou T (1998). Noradrenergic excitation and inhibition of GABAergic cell types in rat frontal cortex. The Journal of neuroscience : the official journal of the Society for Neuroscience 18, 6963–6976. [PubMed: 9712665]

Khiroug L, Giniatullin R, Klein RC, Fayuk D, and Yakel JL (2003). Functional mapping and Ca2+ regulation of nicotinic acetylcholine receptor channels in rat hippocampal CA1 neurons. The Journal of neuroscience : the official journal of the Society for Neuroscience 23, 9024–9031. [PubMed: 14534236]

Krishnamurthy P, Silberberg G, and Lansner A (2015). Long-range recruitment of Martinotti cells causes surround suppression and promotes saliency in an attractor network model. Front Neural Circuits 9, 60. [PubMed: 26528143]

Kuchibhotla KV, Gill JV, Lindsay GW, Papadoyannis ES, Field RE, Sten TA, Miller KD, and Froemke RC (2017). Parallel processing by cortical inhibition enables context-dependent behavior. Nature neuroscience 20, 62–71. [PubMed: 27798631]

Lee MG, Hassani OK, Alonso A, and Jones BE (2005). Cholinergic basal forebrain neurons burst with theta during waking and paradoxical sleep. The Journal of neuroscience : the official journal of the Society for Neuroscience 25, 4365–4369. [PubMed: 15858062]

Levy RB, and Aoki C (2002). Alpha7 nicotinic acetylcholine receptors occur at postsynaptic densities of AMPA receptor-positive and -negative excitatory synapses in rat sensory cortex. The Journal of neuroscience : the official journal of the Society for Neuroscience 22, 5001–5015. [PubMed: 12077196]

Levy RB, and Reyes AD (2012). Spatial profile of excitatory and inhibitory synaptic connectivity in mouse primary auditory cortex. The Journal of neuroscience : the official journal of the Society for Neuroscience 32, 5609–5619. [PubMed: 22514322]

Levy RB, Reyes AD, and Aoki C (2008). Cholinergic modulation of local pyramid-interneuron synapses exhibiting divergent short-term dynamics in rat sensory cortex. Brain Res 1215, 97–104. [PubMed: 18482715]

Lubin M, Erisir A, and Aoki C (1999). Ultrastructural immunolocalization of the alpha 7 nAChR subunit in guinea pig medial prefrontal cortex. Ann N Y Acad Sci 868, 628–632. [PubMed: 10414345]

Manseau F, Marinelli S, Mendez P, Schwaller B, Prince DA, Huguenard JR, and Bacci A (2010). Desynchronization of neocortical networks by asynchronous release of GABA at autaptic and synaptic contacts from fast-spiking interneurons. PLoS Biol 8.

Marguet SL, and Harris KD (2011). State-dependent representation of amplitude-modulated noise stimuli in rat auditory cortex. The Journal of neuroscience : the official journal of the Society for Neuroscience 31, 6414–6420. [PubMed: 21525282]

Markram H, Muller E, Ramaswamy S, Reimann MW, Abdellah M, Sanchez CA, Ailamaki A, Alonso-Nanclares L, Antille N, Arsever S, et al. (2015). Reconstruction and Simulation of Neocortical Microcircuitry. Cell 163, 456–492. [PubMed: 26451489]

McGehee DS, Heath MJ, Gelber S, Devay P, and Role LW (1995). Nicotine enhancement of fast excitatory synaptic transmission in CNS by presynaptic receptors Science (New York, NY 269, 1692–1696. [PubMed: 7569895]

McGinley MJ, Vinck M, Reimer J, Batista-Brito R, Zagha E, Cadwell CR, Tolias AS, Cardin JA, and McCormick DA (2015). Waking State: Rapid Variations Modulate Neural and Behavioral Responses. Neuron 87, 1143–1161. [PubMed: 26402600]

Metherate R, Cox CL, and Ashe JH (1992). Cellular bases of neocortical activation: modulation of neural oscillations by the nucleus basalis and endogenous acetylcholine. The Journal of neuroscience : the official journal of the Society for Neuroscience 12, 4701–4711.

Miller KD (2016). Canonical computations of cerebral cortex. Current opinion in neurobiology 37, 75–84. [PubMed: 26868041]

Ochoa EL, Chattopadhyay A, and McNamee MG (1989). Desensitization of the nicotinic acetylcholine receptor: molecular mechanisms and effect of modulators. Cell Mol Neurobiol 9, 141–178. [PubMed: 2663167]

Pafundo DE, Nicholas MA, Zhang R, and Kuhlman SJ (2016). Top-Down-Mediated Facilitation in the Visual Cortex Is Gated by Subcortical Neuromodulation. The Journal of neuroscience : the official journal of the Society for Neuroscience 36, 2904–2914. [PubMed: 26961946]

Pakan JM, Lowe SC, Dylda E, Keemink SW, Currie SP, Coutts CA, and Rochefort NL (2016). Behavioral-state modulation of inhibition is context-dependent and cell type specific in mouse visual cortex. Elife 5.

Pala A, and Petersen CC (2015). In vivo measurement of cell-type-specific synaptic connectivity and synaptic transmission in layer 2/3 mouse barrel cortex. Neuron 85, 68–75. [PubMed: 25543458]

Parikh V, Kutlu MG, and Gould TJ (2016). nAChR dysfunction as a common substrate for schizophrenia and comorbid nicotine addiction: Current trends and perspectives. Schizophr Res 171, 1–15. [PubMed: 26803692]

Parker JC, Sarkar D, Quick MW, and Lester RA (2003). Interactions of atropine with heterologously expressed and native alpha 3 subunit-containing nicotinic acetylcholine receptors. Br J Pharmacol 138, 801–810. [PubMed: 12642381]

Picciotto MR, Higley MJ, and Mineur YS (2012). Acetylcholine as a neuromodulator: cholinergic signaling shapes nervous system function and behavior. Neuron 76, 116–129. [PubMed: 23040810]

Polack PO, Friedman J, and Golshani P (2013). Cellular mechanisms of brain state-dependent gain modulation in visual cortex. Nat Neurosci 16, 1331–1339. [PubMed: 23872595]

Potjans TC, and Diesmann M (2014). The cell-type specific cortical microcircuit: relating structure and activity in a full-scale spiking network model. Cerebral cortex 24, 785–806. [PubMed: 23203991]

Poulet JF, Fernandez LM, Crochet S, and Petersen CC (2012). Thalamic control of cortical states. Nature neuroscience 15, 370–372. [PubMed: 22267163]

Poulet JF, and Petersen CC (2008). Internal brain state regulates membrane potential synchrony in barrel cortex of behaving mice. Nature 454, 881–885. [PubMed: 18633351]

Puddifoot CA, Wu M, Sung RJ, and Joiner WJ (2015). Ly6h regulates trafficking of alpha7 nicotinic acetylcholine receptors and nicotine-induced potentiation of glutamatergic signaling. The Journal of neuroscience : the official journal of the Society for Neuroscience 35, 3420–3430.

Renart A, de la Rocha J, Bartho P, Hollender L, Parga N, Reyes A, and Harris KD (2010). The asynchronous state in cortical circuits Science (New York, NY 327, 587–590. [PubMed: 20110507]

Reyes A, Lujan R, Rozov A, Burnashev N, Somogyi P, and Sakmann B (1998). Target-cell-specific facilitation and depression in neocortical circuits. Nature neuroscience 1, 279–285. [PubMed: 10195160]

Sanchez-Vives MV, and McCormick DA (2000). Cellular and network mechanisms of rhythmic recurrent activity in neocortex. Nature neuroscience 3, 1027–1034. [PubMed: 11017176]

Seino S, and Shibasaki T (2005). PKA-dependent and PKA-independent pathways for cAMP-regulated exocytosis. Physiol Rev 85, 1303–1342. [PubMed: 16183914]

Silberberg G, and Markram H (2007). Disynaptic inhibition between neocortical pyramidal cells mediated by Martinotti cells. Neuron 53, 735–746. [PubMed: 17329212]

Somjen GG (2004). Ions in the brain: normal function, seizures, and stroke (New York, Oxford University press).

Sun HY, Bartley AF, and Dobrunz LE (2009). Calcium-permeable presynaptic kainate receptors involved in excitatory short-term facilitation onto somatostatin interneurons during natural stimulus patterns. Journal of neurophysiology 101, 1043–1055. [PubMed: 19073817]

Surmeier DJ, Ding J, Day M, Wang Z, and Shen W (2007). D1 and D2 dopamine-receptor modulation of striatal glutamatergic signaling in striatal medium spiny neurons. Trends Neurosci 30, 228–235. [PubMed: 17408758]

Sylwestrak EL, and Ghosh A (2012). Elfn1 regulates target-specific release probability at CA1-interneuron synapses Science (New York, NY 338, 536–540. [PubMed: 23042292]

Tomioka NH, Yasuda H, Miyamoto H, Hatayama M, Morimura N, Matsumoto Y, Suzuki T, Odagawa M, Odaka YS, Iwayama Y, et al. (2014). Elfn1 recruits presynaptic mGluR7 in trans and its loss results in seizures. Nat Commun 5, 4501. [PubMed: 25047565]

Trevino M (2016). Inhibition Controls Asynchronous States of Neuronal Networks. Front Synaptic Neurosci 8, 11. [PubMed: 27274721]

Urban-Ciecko J, and Barth AL (2016). Somatostatin-expressing neurons in cortical networks. Nat Rev Neurosci 17, 401–409. [PubMed: 27225074]

Urban-Ciecko J, Fanselow EE, and Barth AL (2015). Neocortical somatostatin neurons reversibly silence excitatory transmission via GABAb receptors. Current biology : CB 25, 722–731. [PubMed: 25728691]

van Aerde KI, Qi G, and Feldmeyer D (2015). Cell type-specific effects of adenosine on cortical neurons. Cerebral cortex 25, 772–787. [PubMed: 24108800]

Vidal C, and Changeux JP (1993). Nicotinic and muscarinic modulations of excitatory synaptic transmission in the rat prefrontal cortex in vitro. Neuroscience 56, 23–32. [PubMed: 7901807]

Vierling-Claassen D, Cardin JA, Moore CI, and Jones SR (2010). Computational modeling of distinct neocortical oscillations driven by cell-type selective optogenetic drive: separable resonant circuits controlled by low-threshold spiking and fast-spiking interneurons. Front Hum Neurosci 4, 198. [PubMed: 21152338]

Wall NR, De La Parra M, Sorokin JM, Taniguchi H, Huang ZJ, and Callaway EM (2016). Brain-Wide Maps of Synaptic Input to Cortical Interneurons. The Journal of neuroscience : the official journal of the Society for Neuroscience 36, 4000–4009. [PubMed: 27053207]

Yan GM, Lin SZ, Irwin RP, and Paul SM (1995). Activation of muscarinic cholinergic receptors blocks apoptosis of cultured cerebellar granule neurons. Mol Pharmacol 47, 248–257. [PubMed: 7870032]

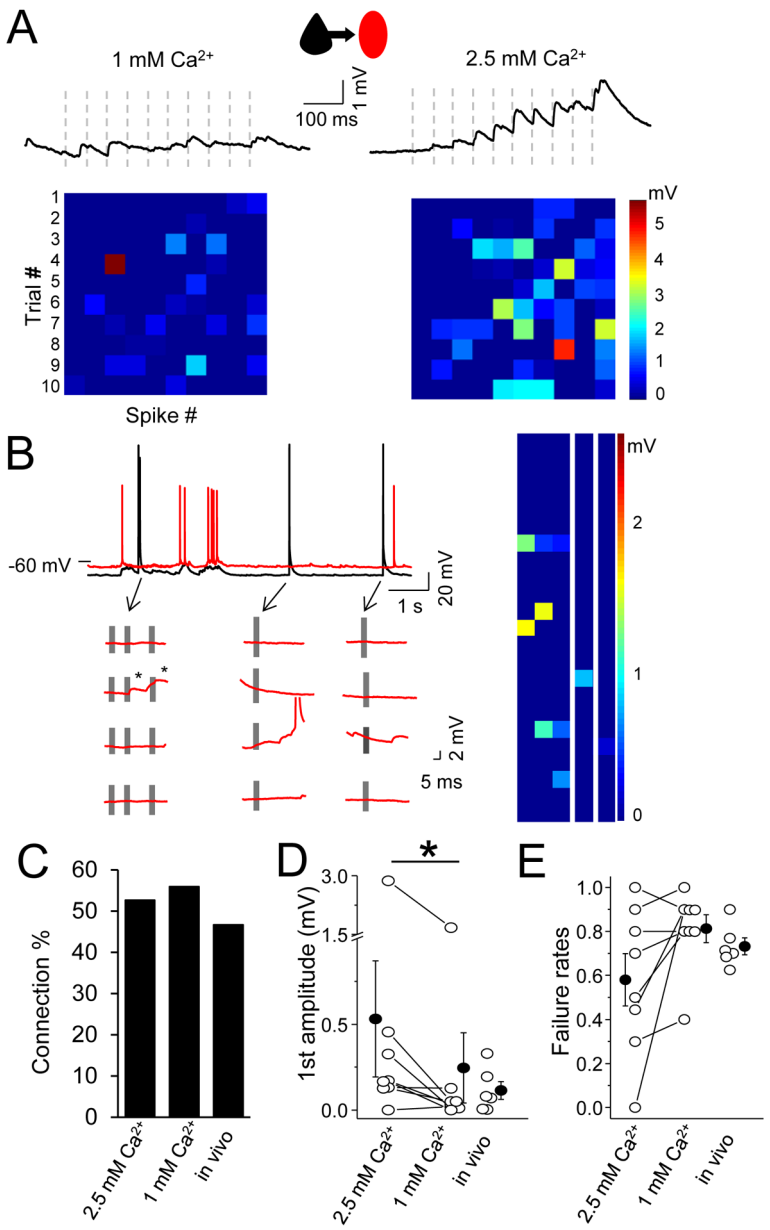

Figure 1. Local excitatory synaptic transmission onto layer 2/3 SST neurons is suppressed by network activity.

(**A**) The averaged trace of 10 response trials for a synaptic connection from a L2/3 pyramidal neuron to an SST interneuron (Pyr-SST) under normal (right) and elevated Ca^{2+} recording conditions. Ten presynaptic spikes (dashed vertical lines) at 20 Hz were delivered. Heatmaps at bottom show response amplitude for 10 trials (columns) with 10 spike pulses each (rows), using a linear scale where red scaled to the maximum amplitude. (**B**) Individual SST (red) response to a naturalistic spike train in pyramidal neuron (black), below 4 subsequent examples at higher time scale. Gray bars indicate individual spikes. Heatmap (right) shows response amplitude for 25, naturalistic spike trials, using a linear scale where red is maximum amplitude. (C) Connection probability in both conditions in slice and *in vivo*. (**D**) Mean EPSP amplitude in response to the first spike in the train, for 1 mM and 2.5 mM Ca^{2+}

conditions in acute brain slice, and *in vivo*. EPSP amplitude is significantly different only between 1 and 2.5 mM Ca^{2+}. (**E**) Mean failure rate after the first spike, for all conditions. For all, open circles represent individual cell measurements and filled circles represent all-cell mean± SEM, respectively (D,E).

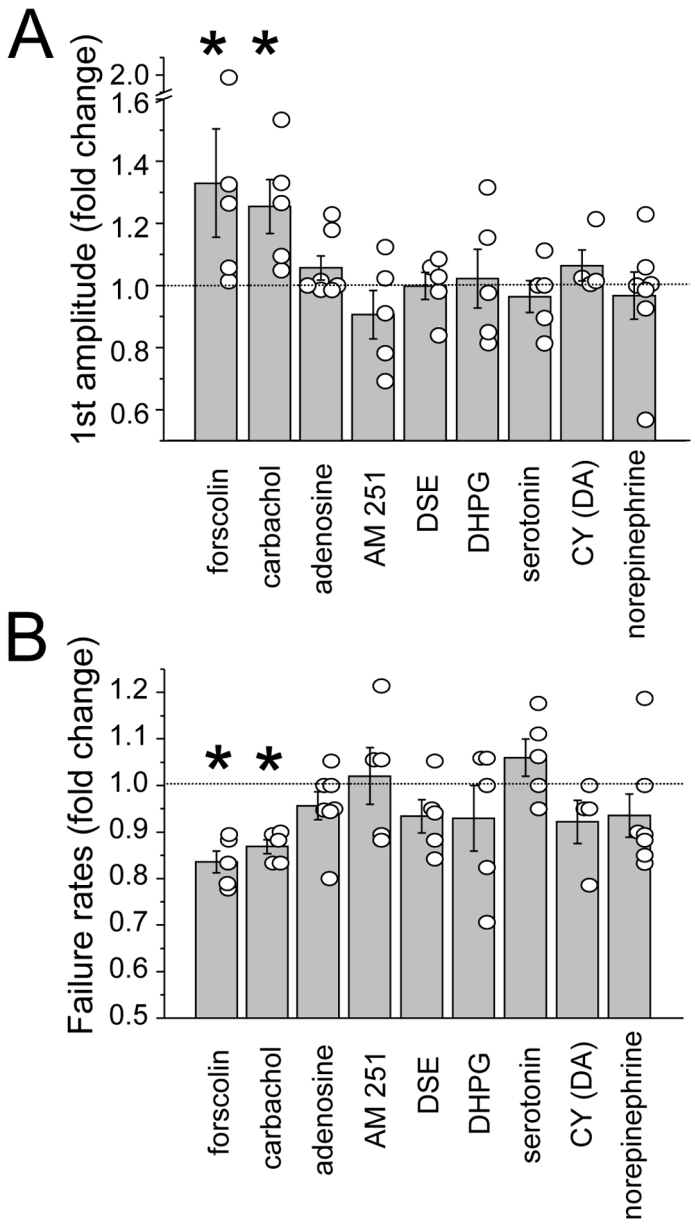

Figure 2. Screening for modulatory systems regulating Pyr-SST synaptic transmission.

(**A**) The -fold change of the first EPSP amplitude in a baseline condition and the following bath-applied agents: forskolin (cell-permeable activator of adenylyl cyclase); carbachol (a broad-spectrum cholinergic agonist), adenosine; AM-251 (endocannabinoid inhibitors); depolarization-induced suppression of excitation (DSE); DHPG (a metabotropic glutamate receptor antagonist); serotonin; CY 208–243 (D1 receptor agonist) and norepinephrine. (B) The -fold change of the mean failure rate for the same conditions as in (**A**). Open circles represent individual cell values; bars represent all-cell mean± SEM.

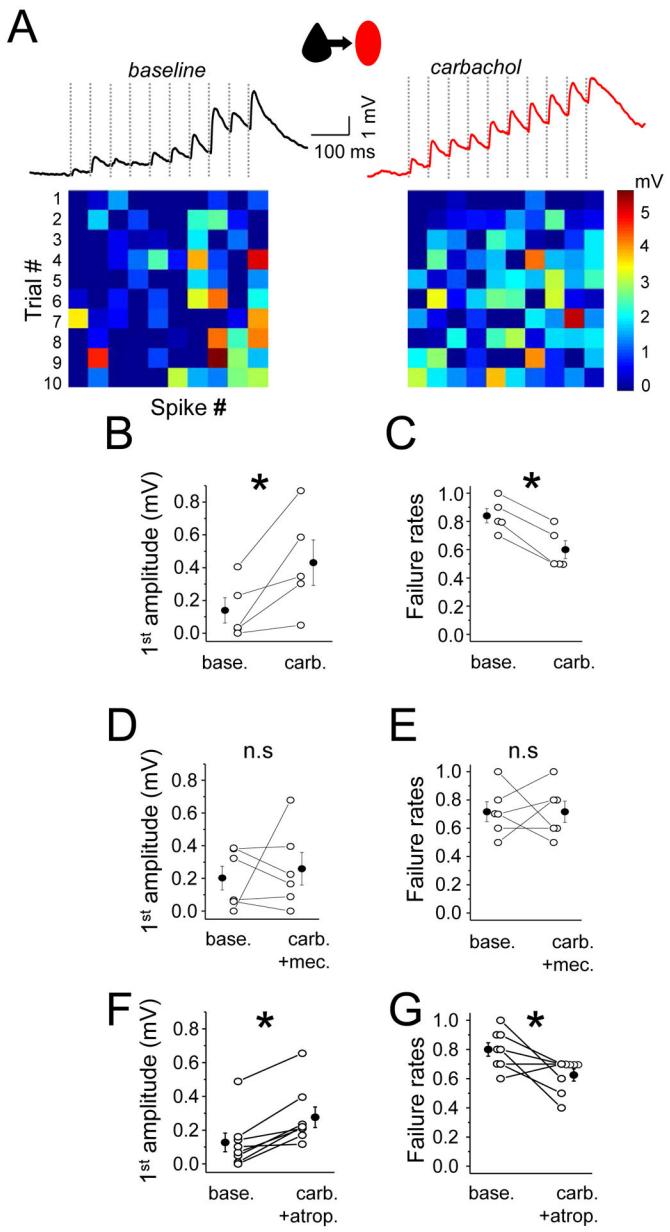

Figure 3. Nicotinic receptors enhance EPSP efficacy onto Pyr-SST connections.

(**A**) The averaged trace of 10 response trials for a Pyr to SST connection under baseline conditions (left) and in carbachol. Ten presynaptic spikes (dashed vertical lines) at 20 Hz were delivered. Heatmaps at bottom show response amplitude as in Figure 1. (**B**) Mean EPSP amplitude in response to the first spike in the train, for baseline and in carbachol conditions. (**C**) Mean failure rate after the first spike, for both conditions. (**D**) and (**E**) The same as in (B) and (C) but with selective nicotinic receptor activation (carbachol and atropine, a muscarinic receptor antagonist). (**F**) and (**G**) The same as in (B) and (C) but with selective muscarinic receptor activation (carbachol and mecamylamine, a nicotinic receptor antagonist). For all, open circles represent individual cell measurements and filled circles represent all-cell mean± SEM, respectively (B-G).

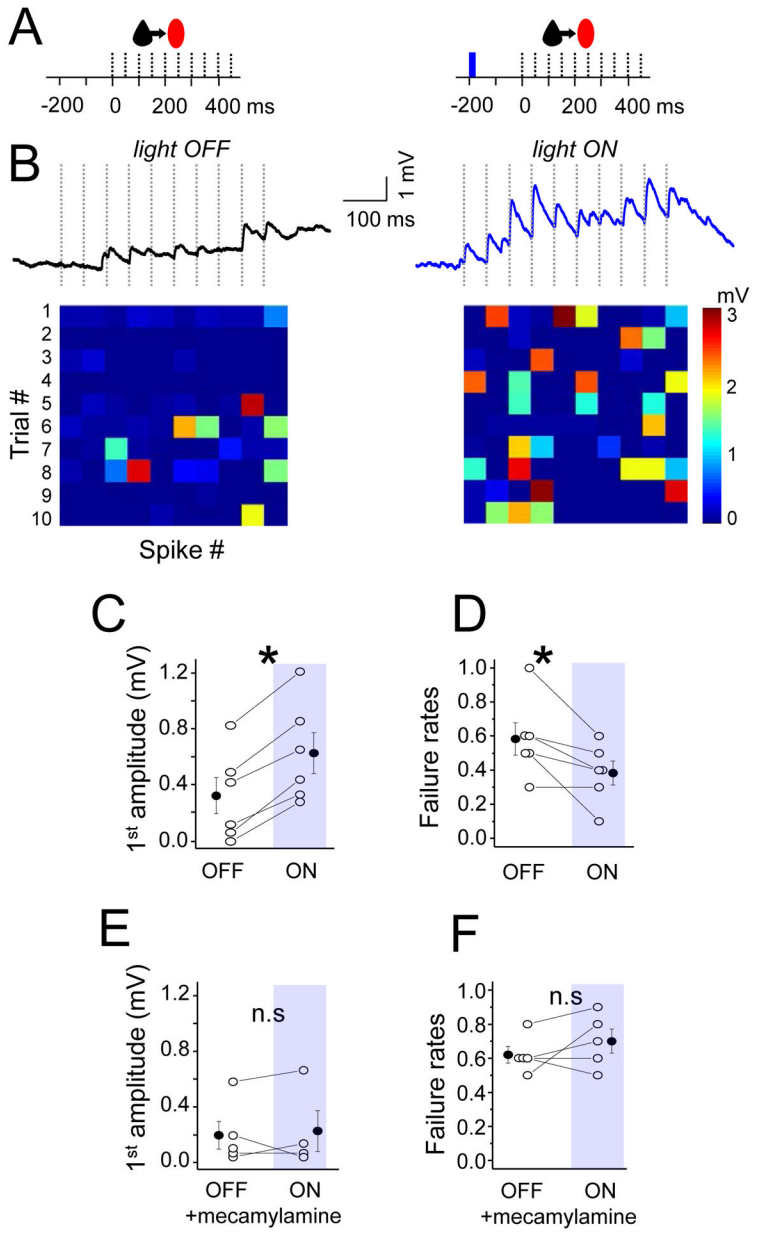

Figure 4. Nicotinic receptors enhance EPSP efficacy at Pyr-SST connections.

(**A**) Schematic of the stimulation protocol. 1-single blue light (10 ms) was delivered 200 ms prior to the presynaptic spike train. (**B**) The averaged trace of EPSP under baseline/light OFF and light ON conditions. Heatmaps at bottom show response amplitude for both conditions as described in previous figures. (**C**) Mean EPSP amplitude in response to the first spike in the train, for both conditions. (**D**) Mean failure rate after the first spike, for both conditions. (**E**) and (**F**) The same as (C) and (D) but in the presence of the nicotinic receptors antagonist (mecamylamine). For all, open circles represent individual cell measurements and filled circles represent all-cell mean± SEM, respectively (C-F). See also Figure S1 and S2.

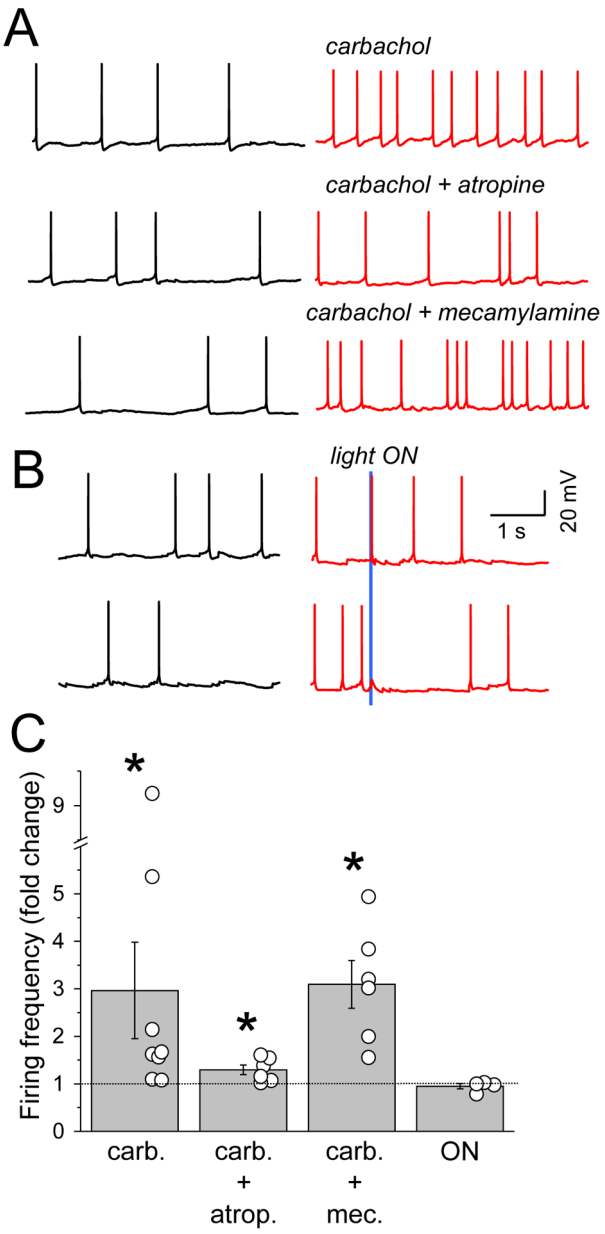

Figure 5. SST neuron spontaneous firing with pharmacological and optogenetic ACh receptor activation.

(A) Firing frequency in baseline and in the presence of carbachol, carbachol and atropine, carbachol and mecamylamine. **(B)** The example traces showing the spike (top) and depolarization (bottom) of SST neurons in response to 10 ms-single light stimulation. **(C)** Mean fold change in spontaneous firing frequency for different conditions: carbachol, carbachol and atropine, carbachol and mecamylamine, light ON. The bar graphs represent mean±SEM.

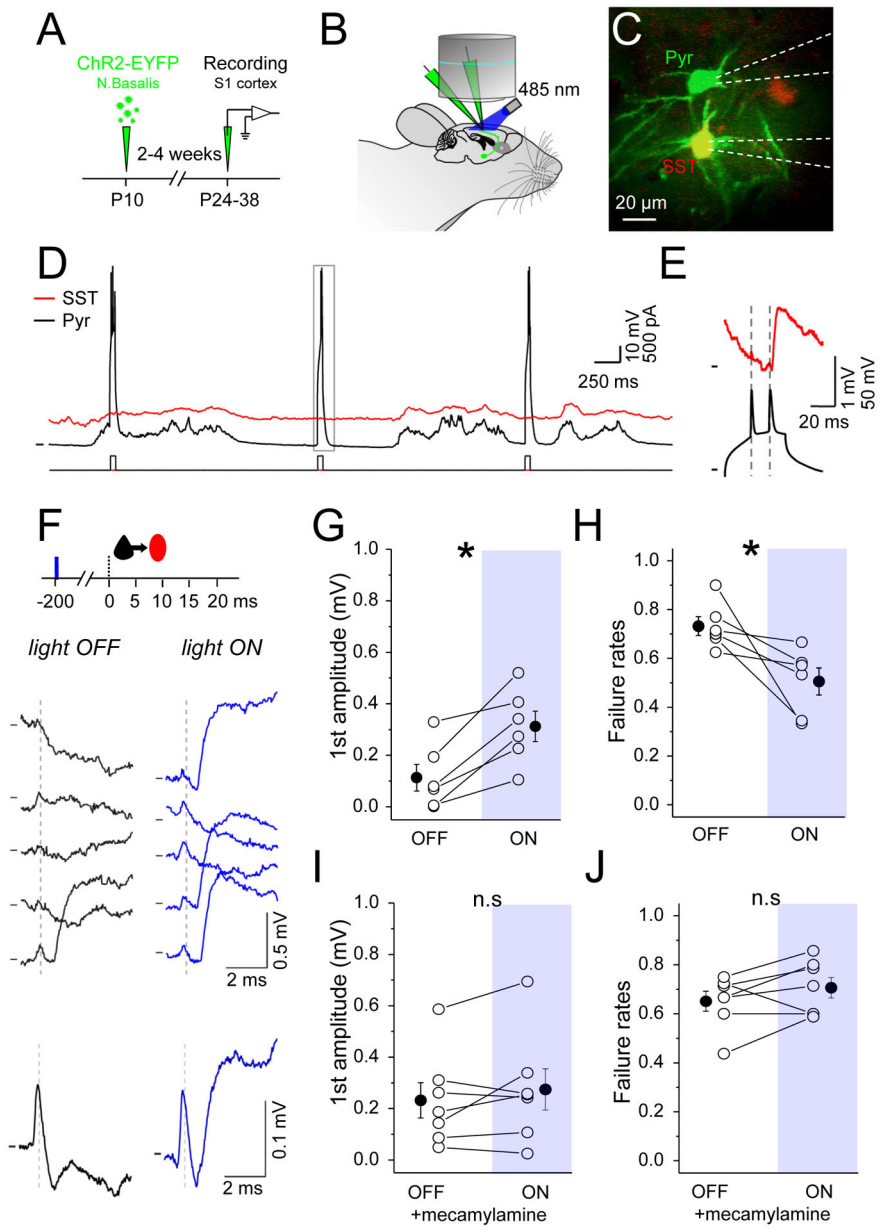

Figure 6. Nicotinic receptors enhance EPSP efficacy at Pyr-SST connections *in vivo*.

(**A**) Schematic of the experimental procedure. P10 SST-IRES-Cre-Ai9 pups were injected in nucleus basalis (Bregma: 0.02 mm, lat: 1.3 mm, depth: 4.5 mm). After an incubation period of 2–4 weeks mice were anesthetized and electrophysiological recordings were performed in somatosensory cortex. (**B**) Schematic of the recording setup. (**C**) *In vivo* 2-photon image of a pyramidal neuron (green cell soma) connected to a SST interneuron (yellow cell soma). White dashed lines show recording electrodes outlines. (**D**) Example recording of a Pyr (black trace) connected to SST (red trace). Bottom trace shows injected current into Pyr to drive spiking. (**E**) Zoom of the grey rectangle in (D). In this example two spikes were evoked and only the second one led to an EPSP in the SST interneuron (red trace). (**F**) Top: schematic of the experimental protocol: 1 blue light pulse (10 ms) was delivered on the brain

surface (5-15 mm) 200 ms prior to the presynaptic Pyr doublet of spikes. Middle: example single traces showing the SST response to the first evoked Pyr spike under baseline/light OFF (black traces) and light ON (blue traces) conditions. Bottom: average responses from the above Pyr to SST connection (Light OFF, n=27 trials; Light ON, n=30 trials). (**G**) Mean EPSP amplitude in response to the first spike of the doublet, for both conditions. (**H**) Mean failure rate after the first spike, for both conditions. (**I**) and (**J**) The same as (G) and (H) but in the presence of the nicotinic receptors antagonist (mecamylamine). See also Figure S3 and S4.

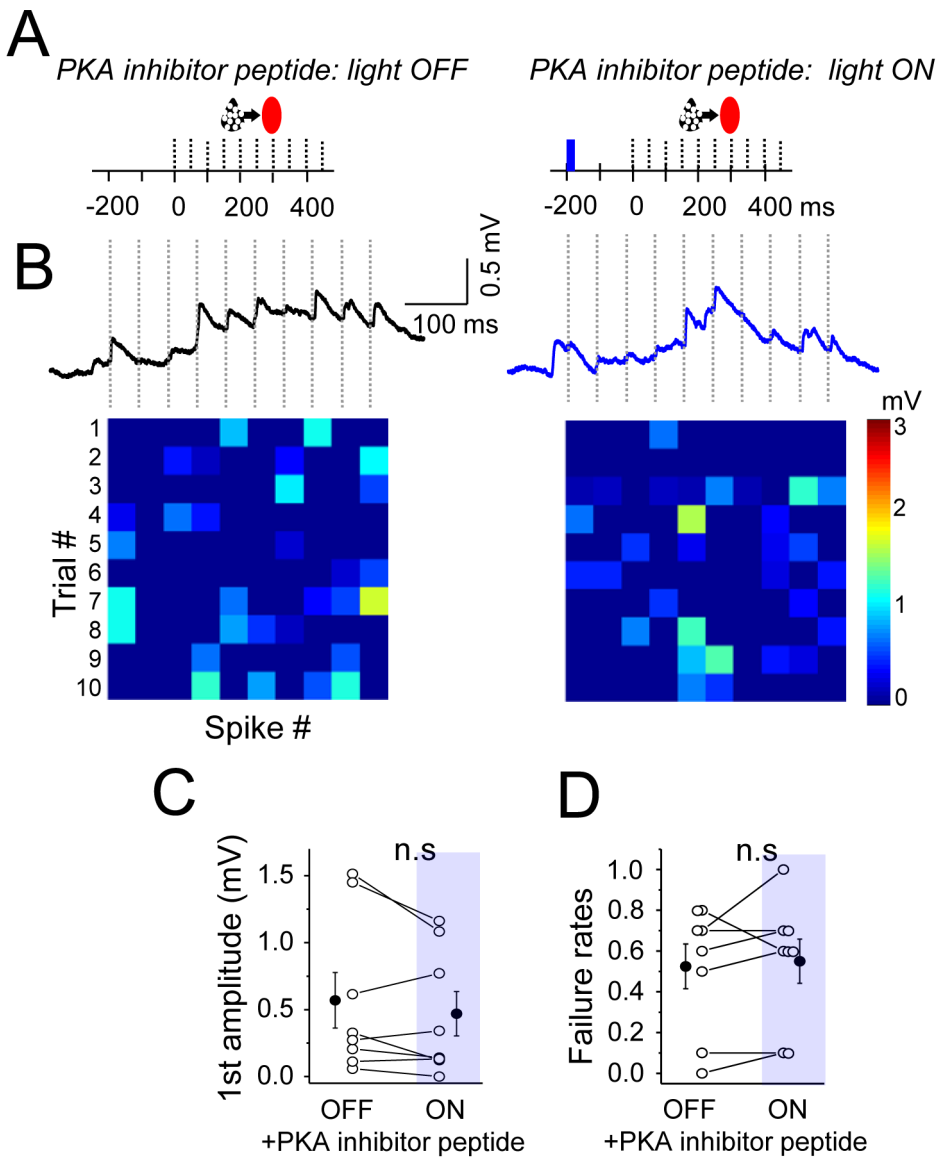

Figure 7. Presynaptic inhibition of PKA eliminates ACh-enhancement of Pyr-SST synapses.

(A) Schematic of the stimulation protocol. 1-single blue light (10 ms) was delivered 200 ms prior to the presynaptic spike train in the presence of PKA inhibitor peptide in the presynaptic Pyr cell. (**B**) The averaged trace of EPSP under baseline/light OFF and light ON conditions. Heatmaps at bottom show response amplitude for both conditions as described in previous figures. (**C**) Mean EPSP amplitude in response to the first spike in the train, for both conditions. (**D**) Mean failure rate after the first spike, for both conditions. For all, open circles represent individual cell measurements and filled circles represent all-cell mean± SEM, respectively (C,D). See also Figure S5.

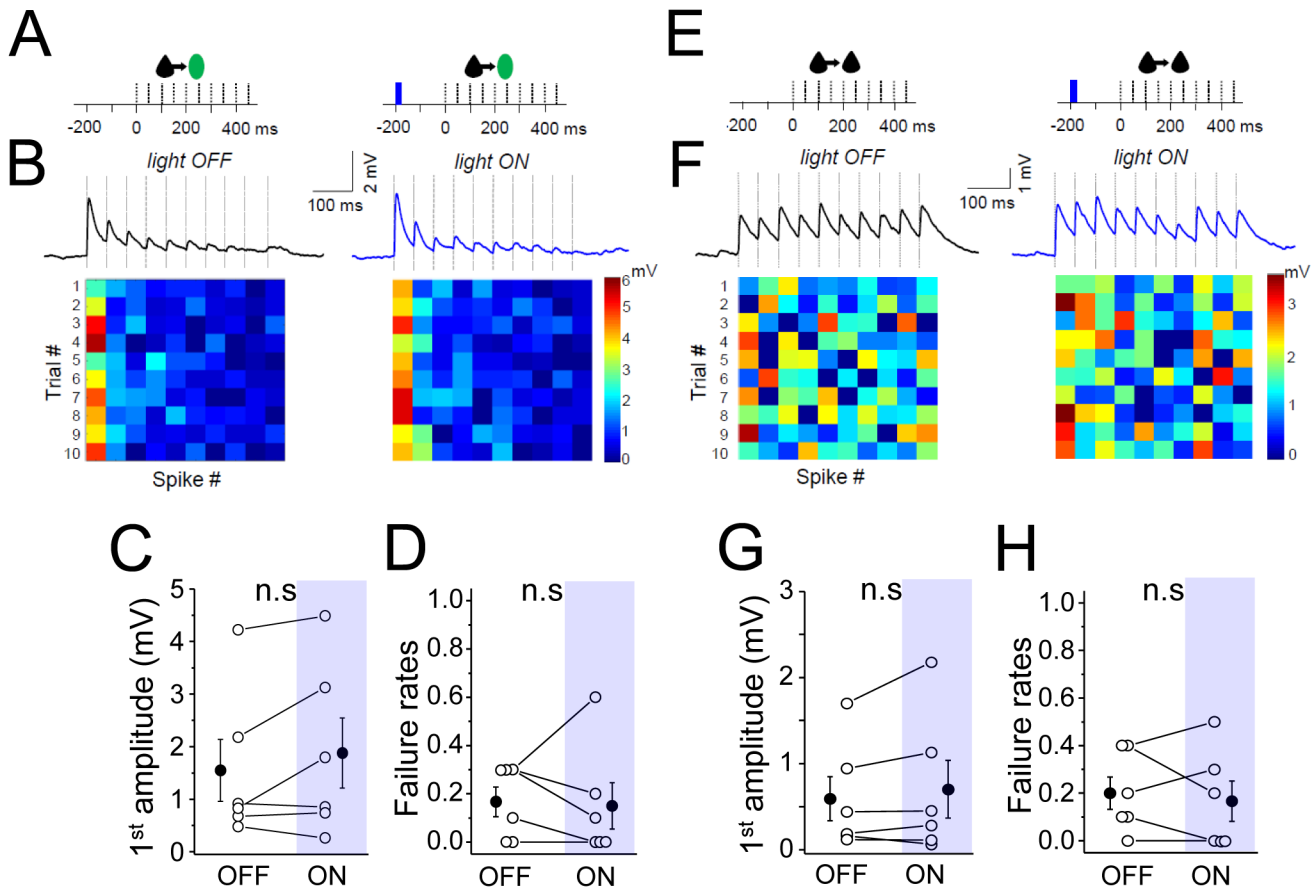

Figure 8. Pyr-PV and Pyr-Pyr connections are not enhanced during optogenetically driven ACh release.

(**A**) Schematic of the stimulation protocol for Pyr-PV connections. 1-single blue light (10 ms) was delivered 200 ms prior to the presynaptic spike train. (**B**) The averaged trace of EPSP under baseline/light OFF and light ON conditions. Heatmaps at bottom show response amplitude for both conditions as described in previous figures. (**C**) Mean EPSP amplitude in response to the first spike in the train, for both conditions. (**D**) Mean failure rate after the first spike, for both conditions. See also Figure S6. (**E**) Schematic of the stimulation protocol for L2 Pyr-Pyr connections. 1-single blue light (10 ms) was delivered 200 ms prior to the presynaptic spike train. (F) The averaged trace of 10 response trials for Pyr-Pyr connection under baseline condition (left) and in carbachol. Ten presynaptic spikes (dashed vertical lines) at 20 Hz were delivered. Heatmaps at bottom show response amplitude for 10, 10 spike trials, using a linear scale where red is maximum amplitude in both conditions. (G) Mean EPSP amplitude in response to the first spike in the train, for baseline/light OFF and light ON conditions. (H) Mean failure rate after the first spike, for both conditions. For all, open circles represent individual cell measurements and filled circles represent all-cell mean ± SEM, respectively (C,D and G.H). See also Figure S7.

KEY RESOURCES TABLE

REAGENT or RESOURCE	SOURCE	IDENTIFIER
Antibodies		
Chicken anti-GFP	Abcam	ab113970
Rabbit anti-VAChT	Synaptic System	Sysy 139103
alexaFluor 488 goat anti-chicken	ThermoFisher	A11039
AlexaFluor 647 goat anti-Rabbit	ThermoFisher	A21245
Bacterial and Virus Strains		
AVV9.CAG.flex.tdTomato	Penn Vector Core	AV-9-ALL864
AVV9.CAG.flex.mCherry	UNC Vector Core	n/a
AAV9/2.CamKII.ChR2(T159C)-p2A.EYFP	Charité Vector Core	VCA-13
VSVG.HIV.SIN.Synapsin.ChR2(H134R).EYFP.WP	Charité Vector Core	BLV-679
Biological Samples		
Chemicals, Peptides, and Recombinant Proteins		
forskolin	Tocris	Cat#1099
rolipram	Sigma	Cat# R6520
norepinephrine	Sigma	Cat# A7257
carbachol	Sigma	Cat# C4382
mecamylamine	Sigma	Cat# M9020
atropine	Sigma	Cat# 0257
serotonin	Tocris	Cat# 3543
CY 208–243	Tocris	Cat# 1249
adenosine	Sigma	Cat# A9251
AM 251	Tocris	Cat#1117
DHPG	Sigma	Cat# G2536
PKA inhibitor fragment PKI	Tocris	Cat#1904
AlexaFluor 594	ThermoFisher	Cat#A10438
DAPI Fluoromount-G	SouthernBiotech	0100–20
Critical Commercial Assays		
Deposited Data		
Experimental Models: Cell Lines		

REAGENT or RESOURCE	SOURCE	IDENTIFIER
Experimental Models: Organisms/Strains		
Mouse-C57BL/6J	Jaxon Lab	#000664
Mouse-SST-IRES-Cre	Jaxon Lab	#013044
Mouse-Ai14	Jaxon Lab	#007908
Mouse-Ai9	Jaxon Lab	#007909
Mouse-Ai3	Jaxon Lab	#007903
Mouse-ChAT-ChR-YFP-BAC	Jaxon Lab	#014545
Mouse-PValb-2A-Cre	Jaxon Lab	#013044
Oligonucleotides		
Recombinant DNA		
Software and Algorithms		
Igor Pro 6	Wavemetrics	www.wavemetrics.com
Matlab	MathWorks	www.mathworks.com
Instat (Demo)	GraphPad	www.graphpad.com
Other		